73N14925

NASA TECHNICAL NOTE

NASA TN D-7104

NASA TN D-7104

HEAT-TRANSFER AND PRESSURE DISTRIBUTIONS ON HEMISPHERE-CYLINDERS IN METHANE-AIR COMBUSTION PRODUCTS AT MACH 7

by Irving Weinstein

Langley Research Center
Hampton, Va. 23365

NATIONAL AERONAUTICS AND SPACE ADMINISTRATION • WASHINGTON, D. C. • JANUARY 1973

1. Report No.	2. Government Accession No.	3. Recipient's Catalog No.
NASA TN D-7104		

4. Title and Subtitle
HEAT-TRANSFER AND PRESSURE DISTRIBUTIONS ON HEMISPHERE-CYLINDERS IN METHANE-AIR COMBUSTION PRODUCTS AT MACH 7

5. Report Date
January 1973

6. Performing Organization Code

7. Author(s)
Irving Weinstein

8. Performing Organization Report No.
L-8359

9. Performing Organization Name and Address
NASA Langley Research Center
Hampton, Va. 23365

10. Work Unit No.
501-22-06-01

11. Contract or Grant No.

12. Sponsoring Agency Name and Address
National Aeronautics and Space Administration
Washington, D.C. 20546

13. Type of Report and Period Covered
Technical Note

14. Sponsoring Agency Code

15. Supplementary Notes

16. Abstract

Heat-transfer and pressure distributions were measured over the surfaces of three hemisphere-cylinder models tested at a nominal Mach number of 7 in the Langley 8-foot high-temperature structures tunnel which uses methane-air products of combustion as a test medium. The results showed that the heat-transfer and pressure distributions over the surface of the models were in good agreement with experimental data obtained in air and also with theoretical predictions.

17. Key Words (Suggested by Author(s))
Hypersonic flow
Methane-air combustion products
Hemisphere-cylinder
Convective heat transfer
Pressure distribution

18. Distribution Statement
Unclassified – Unlimited

19. Security Classif. (of this report)	20. Security Classif. (of this page)	21. No. of Pages	22. Price*
Unclassified	Unclassified	38	$3.00

*For sale by the National Technical Information Service, Springfield, Virginia 22151

HEAT-TRANSFER AND PRESSURE DISTRIBUTIONS ON HEMISPHERE-CYLINDERS IN METHANE-AIR COMBUSTION PRODUCTS AT MACH 7

By Irving Weinstein
Langley Research Center

SUMMARY

An experimental investigation was conducted to evaluate the use of a combustion-product test medium for obtaining aerodynamic heating and loading data on large models. Three hemisphere-cylinder models were tested at angles of attack up to 18° in the Langley 8-foot high-temperature structures tunnel, which uses methane-air combustion products as the test medium. The tests were conducted at stagnation temperatures from 1400 K to 2056 K (2520° R to 3700° R) and free-stream unit Reynolds numbers from 1.3×10^6 to 4.6×10^6 per meter (0.4×10^6 to 1.4×10^6 per foot). The tunnel nominal free-stream Mach number was 7.0.

The results of tests at angles of attack from 0° to 18° showed that the longitudinal pressure distributions obtained over the surface of the models were in good agreement with data obtained in air and with theoretical predictions. Measured stagnation-point heating rates were within 7 percent of the theoretical value. Experimental heating distributions obtained at an angle of attack of 0° were also in good agreement with those obtained in air and predicted by theory.

INTRODUCTION

Aerodynamic test facilities that can simulate the heating and loading encountered in flight are indispensable tools for developing structural technology for supersonic and hypersonic vehicles. For effective structural testing, these facilities must accommodate large structural components and must provide a realistic aerothermal environment. The Langley 8-foot high-temperature structures tunnel is a large hypersonic wind tunnel which was designed specifically for such testing. This facility provides an aerothermal environment representative of Mach 7 flight by burning methane under high pressure in air and using the resulting combustion products as a test medium.

Although the use of combustion products as a test medium was previously explored in a small combustion facility (ref. 1), it was necessary to evaluate the test stream of the present facility to establish its suitability for aerothermally testing large models. Accordingly, aerodynamic heating and pressure distributions were measured on three hemisphere-cylinder models up to 61 cm (24 in.) in diameter. The models were tested at angles of attack up to 18°, at stagnation temperatures from 1400 K to 2056 K (2520° R to 3700° R), and at free-stream Reynolds numbers from 1.3×10^{6} to 4.6×10^{6} per meter (0.4×10^{6} to 1.4×10^{6} per foot). The measured distributions presented herein are compared with other distributions obtained in air and those predicted by theory.

SYMBOLS

The units used for physical quantities defined in this paper are given both in the International System of Units (SI) and in the U.S. Customary Units. The calculations were made in U.S. Customary Units. Factors relating the two systems are given in reference 2 and in the appendix.

c	specific heat of material, J/kg-$^{\circ}$K (Btu/lb-$^{\circ}$R)
M	Mach number
p	pressure, N/m^2 (lb/in^2)
q	dynamic pressure, N/m^2 (lb/ft^2)
$\dot{q}$	heating rate, W/m^2 (Btu/ft^2-sec)
R	free-stream Reynolds number based on model diameter
r	model nose radius, m (ft)
s	distance along model surface measured from stagnation point, m (ft)
$\bar{s}$	distance along model measured from axis of symmetry, m (ft)
T	temperature, K ($^{\circ}$R)
t	time, sec
α	angle of attack, deg

β	meridian angle, deg
δ	standoff distance of bow shock wave
θ	angle between model axis and inward normal to surface, deg
ρ	material density, g/m^3 (lb/ft^3)
τ	model skin thickness, m (ft)

Subscripts:

l	local static conditions
s	model stagnation point
t	total conditions
∞	free-stream conditions

MODELS

Three hemisphere-cylinder models were used for this investigation. One of the models was used for both heat-transfer and pressure measurements; a second model was used for pressure measurements only; and a third model was used for heat-transfer measurements only. These models are designated as models A, B, and C, respectively, and are described in subsequent sections.

Model A

A sketch of model A and a photograph of the model mounted in the test section of the Langley 8-foot high-temperature structures tunnel are shown in figure 1. The model, which was 30.48 cm (12.00 in.) in diameter and 0.9 m (36 in.) long, was constructed of 347 stainless steel with a wall thickness of 0.24 cm (0.094 in.) and a surface finish of 0.4 μm (16 μin.) root mean square.

The model was instrumented with twenty-four 0.152-cm-diameter (0.060 in.) surface pressure orifices (see table in fig. 1) which were arranged in a spiral to reduce possible interference effects. The orifices were connected to pressure transducers located within the model cavity with short lengths, 0.3 to 1.2 m (1 to 4 ft), of stainless-steel tubing to minimize the response time of the transducers. The model was also instrumented with 31 chromel-alumel thermocouples of No. 30 wire which were welded to the back surface of the model skin. All but two of these thermocouples were located in the vertical plane of symmetry.

Model B

A sketch of model B and a photograph of the model in the tunnel test section are shown in figure 2. The model, which was 61 cm (24 in.) in diameter and 91 cm (36 in.) long, was constructed of a mild carbon steel and had a wall thickness of 1.3 cm (0.5 in.) and a surface finish of 1.6 μm (63 μin.) root mean square.

The model was instrumented with eleven 0.152 cm (0.060 in.) inside diameter pressure orifices which were located as shown in the table of figure 2. The orifices were connected to pressure transducers which were located inside the model to reduce the tubing length; as a result, a more rapid pressure response occurs.

Model C

A sketch and a photograph of model C are shown in figure 3. This model, which was 35.7 cm (14.06 in.) in diameter and 57 cm (22.5 in.) long, was made of Inconel and had a wall thickness of 0.08 cm (0.031 in.) and a surface finish of 0.4 μm (16 μin.) root mean square.

The model was instrumented with 26 chromel-alumel thermocouples of No. 30 gage wire with each leg resistance welded separately to the back surface of the model skin. All but two of these thermocouples were located in the vertical plane of symmetry.

APPARATUS AND TEST PROCEDURES

Facility

The present investigation was conducted in the Langley 8-foot high-temperature structures tunnel. A schematic drawing of this facility is shown in figure 4. A brief description and operating conditions of this tunnel are reported in references 3 and 4. The facility is a hypersonic blowdown wind tunnel that burns methane in air under high pressure to produce the high energy gases required for simulation of the aerothermal flight environment. The resulting products of combustion are expanded through an axisymmetric contoured nozzle having an exit diameter of 2.4 m (8 ft). The nozzle provides essentially parallel flow at a nominal Mach number of 7 in an open jet test section. A single-stage annular air ejector located downstream of the test section is used to establish supersonic flow and to permit operation at low stagnation pressures. The tunnel test section is 4.3 m (14 ft) long and has a usable test core approximately 1.2 m (4 ft) in diameter. Models are sting mounted on an elevator which inserts the model into the stream after test conditions are established. A model-pitching system provides for angles of attack from -20° to 20°.

The tunnel can be operated over a total temperature range from approximately 1389 K to 2111 K (2500° R to 3800° R). The dynamic-pressure range of the tunnel is from 14 kN/m^2 to 86 kN/m^2 (300 lb/ft^2 to 1800 lb/ft^2) and the free-stream Reynolds number range is 1.1×10^6 to 9.8×10^6 per meter (0.35×10^6 to 3.0×10^6 per foot). These conditions simulate the hypersonic flight environment in the altitude range between 25 km and 40 km (80 000 ft and 130 000 ft).

The facility is equipped with a Z-shaped single-pass schlieren flow-visualization system which can be traversed longitudinally along the test section. The field of view is 0.6 m (2 ft) in diameter, and the mirrors are paraboloidal and have a focal length of 6 diameters. The high-intensity light source uses a xenon X-75 compact arc lamp which can be operated in either a continuous or flash mode.

Test Procedure

After equilibrium flow conditions were established in the tunnel, the models were elevated to the stream center line within 1 second to provide essentially a step-function exposure to the test conditions. The heat-transfer models (models A and C) were tested only at an angle of attack of 0° and were withdrawn from the stream after about 8 seconds to prevent overheating of the thin walls. The pressure distribution model B was inserted at 0° and then pitched to the desired angle where it was allowed to dwell for approximately 5 seconds to allow transducer outputs to stabilize before it was pitched to the next angle. The angle-of-attack range was from 0° to approximately 18°.

The test data were obtained over a model stagnation pressure range from 28 to 96 kN/m^2 (4 to 14 psia) at total temperatures from approximately 1400 K to 2056 K (2520° R to 3700° R). These conditions correspond to free-stream unit Reynolds numbers of 1.3×10^6 to 4.6×10^6 per meter (0.4×10^6 to 1.4×10^6 per foot).

Data Reduction

Outputs of thermocouples and pressure transducers were recorded on the Langley central data recording system at a sampling rate of 20 frames per second. Free-stream conditions in the test section were obtained from conditions measured in the combustor by using the results of previous test-section surveys.

The local convective heating rates were obtained by using the one-dimensional transient thin-wall technique which equates the heat entering the surface to the heat stored so that $\dot{q}_l = \rho c \tau \frac{dT}{dt}$. The temperature rise rate dT/dt was evaluated at a time when the model reached the center line of the test stream, which occurred at approximately the time of maximum temperature rise rate. At that time, the surface temperature was low, averaging about 344 K (620° R) at the stagnation point and 306 K (550° R) on the cylinder. Consequently, heat conduction through and along the wall and heat lost by radiation from the surface were considered to be negligible.

Pressure distributions were normalized by using measured stagnation point pressures. Since model A had no pressure orifice at the stagnation point, Newtonian theory was used to derive the stagnation pressure from the pressure measured at $\theta = 5^\circ$. The thermal, transport, and flow properties of methane-air combustion products of reference 5 were used in reducing all data and in computing theoretical values.

Accuracy

Accuracies of the parameters presented are estimated to be generally within the following limitations:

Mach number, M_∞	± 0.1
Model stagnation pressure, p_s, percent	± 2
Dynamic pressure, q, percent	± 5
Local convective heating rate, $\dot{q}$, percent	± 6
Total temperature, T_t, K ($^\circ$R)	± 42 (± 75)
Angle of attack, α, deg	± 0.1
Shock standoff distance, δ, percent	± 6

RESULTS AND DISCUSSION

Test conditions for all models and measured stagnation pressures and heating rates are presented in table I.

Pressure Distribution

Values of the nondimensional pressures obtained from model A are presented in table II and are plotted in figure 5. Figures 5(a) and 5(b) present the data obtained at the higher temperatures from 1833 K to 2056 K (3300° R to 3700° R), whereas figures 5(c) and 5(d) show the distributions obtained at the lower temperature range from 1400 K to 1472 K (2520° R to 2650° R). The theoretical curves shown were obtained with the aid of the computer program described in reference 6 which uses a blunt-body solution in the region of subsonic and transonic local velocities, and the method of characteristics where the local velocities are supersonic. The program was modified to include the thermodynamic and transport properties of methane-air combustion gases; however, comparative calculations indicate that the use of combustion gas properties produces only about a 1-percent change in the distributions and in the absolute pressure level at the stagnation point. Variations of the test conditions for a given part of figure 5 produced less than a 2-percent change in the calculated distributions; consequently, a single representative theoretical curve is presented in each part of the figure. The theoretical and experimental distributions are in good agreement over the surface of the model for the low-temperature cases of figures 5(c) and 5(d), the maximum variation of only 8 percent occurring at the aft end of the cylinder. The variation was greater for the higher temperature tests, the theory underpredicting the pressures by a maximum of 25 percent at the aft end of the cylinder (fig. 5(a)).

The pressure distribution range for the tests of model A are compared in figure 6 with data obtained on other hemisphere-cylinder models tested in air at Mach numbers from 4.63 to 8.10. The present data are in very good agreement with all the data obtained in air from references 7 and 8 over the surface of the hemisphere and are bracketed by the data of reference 8 at Mach numbers of 6.03 and 8.10 along the entire length of the cylinder.

Pressure distributions for model B at angles of attack up to about 18° are shown in figure 7. The data presented were obtained from orifices along the windward meridian of the model. The theoretical results were obtained by using the method of reference 6 by treating the hemisphere-cylinder as a spherically blunted cone with a half-angle equal to the model angle of attack. Although this simplified approach does not account for cross-flow effects, the theoretical and experimental distributions are in good agreement. Fairings of data along the cylinder obtained from reference 9 in air at a Mach number of 10.05 for angles of 0°, 10°, and 15° and presented in this figure are also in good agreement with the present data.

Heating Distributions

The experimental stagnation-point heating rates for model A, listed in table I, are compared with theoretical values in figure 8. The theoretical values were obtained from the viscous solution of reference 6 which is based on the stagnation-point solution of Fay and Riddell (ref. 10) and altered to include the properties of combustion products. The solid line represents the condition where theory equals experiment and the dashed lines show a ±5-percent variation with theory. The theory predicts the experimental data very well and is within 7 percent for all the present test data.

Nondimensionalized heating-rate distributions $\dot{q}/\dot{q}_s$ for model A are listed in table III and are presented in figure 9. The theoretical curves on these plots are based on combustion products properties and were obtained with the aid of the computer program of reference 6 which used the laminar boundary-layer solution of Cohen (ref. 11) to obtain the heating rates over the model surface. A single theoretical curve represents all the data on each part of this figure. It can be seen that the experimental data and the theory for model A are in very good agreement over the entire surface of the model except at the aft end of the cylinder at the highest Reynolds number where the heating is underpredicted by laminar theory by approximately 19 percent. This variation may be the effect of transitional flow at the higher Reynolds number.

The heating distributions for model C are listed in table IV and presented in figure 10. The data show some scatter but are generally in good agreement with the theory of reference 6. A comparison of the nondimensional heating distributions for this model with those of model A at comparable test conditions indicates no apparent effect of model wall thickness.

A correlation of heating distributions obtained in combustion products with those obtained in air is shown in figure 11. Typical nondimensional heating distributions for models A and C are shown to be in reasonable agreement with combustion products data from reference 1 and with the theory of reference 6. These data show no significant effect of model diameter on the nondimensional heating distribution along the model surface even though the stagnation-point heating rate is higher for the model with the smaller radius. Therefore, if the heating at the stagnation point is known, the heating along the entire model surface can be predicted. Data obtained in air (from ref. 1) are shown as the solid symbols in figure 11. It can be seen that heating distributions obtained in a combustion-products test medium are in good agreement with those obtained in air and with those predicted by theory.

Flow Patterns

Typical schlieren photographs are shown in figure 12 for tests of model A at three different Reynolds numbers. No perceptible differences in the bow-shock shapes are indicated. The shock-standoff distances measured from enlargements of these photographs are presented in figure 13 and are compared with other experimental data and with theory. The experimental data show that the shock-standoff distance was somewhat less in combustion products than in air but within the range predicted by the theories of references 12 to 14 for air. The standoff distances predicted by the theory of reference 6 using the properties of methane-air combustion products are in good agreement with the experimental data of the present test.

CONCLUDING REMARKS

Heat-transfer and pressure distributions were obtained on three hemisphere-cylinder models in a test medium consisting of methane-air combustion products in the Langley 8-foot high-temperature structures tunnel. Data were obtained at total temperatures from approximately 1400 K to 2056 K (2520° R to 3700° R) for free-stream Reynolds numbers from 1.3×10^6 to 4.6×10^6 per meter (0.4×10^6 to 1.4×10^6 per foot). The tests were made at a nominal Mach number of 7.0.

Pressure distributions over the surface of the model at an angle of attack of 0° and along the windward meridian at angles of attack up to 18° were generally in good agreement with data obtained in air and with theoretical predictions. For all cases the agreement between theory and experiment was very good over the hemisphere whereas the agreement along the cylinder was dependent upon the test conditions. The maximum variations, which occurred at the aft end of the cylinder, ranged from an underprediction by the theory of approximately 25 percent at higher temperatures to an overprediction of approximately 8 percent at the lower temperatures.

Measured stagnation-point heating rates were within 7 percent of the theoretical values. Heating distributions obtained at an angle of attack of 0° were in very good agreement with results obtained in air and with theoretical predictions except for a small region near the aft end of the cylinder. In this region the heating was underpredicted by a maximum of 19 percent and occurred at the higher values of Reynolds numbers of the tests. The flow condition was believed to be transitional.

Langley Research Center,
National Aeronautics and Space Administration,
Hampton, Va., November 21, 1972.

APPENDIX

CONVERSION OF U.S. CUSTOMARY UNITS TO SI UNITS

Factors required for converting U.S. Customary Units to the International System of Units (SI) are given in the following table:

Physical quantity	U.S. Customary Unit	Conversion factor (*)	SI Unit (**)
Heat flux	Btu/ft^2-sec	11 348.9	$watts/meter^2$ (W/m^2)
Length	in.	0.0254	meter (m)
	per ft	3.28	per meter (m^{-1})
Pressure	lbf/in^2	6894.757	$newtons/meter^2$ (N/m^2)
	lbf/ft^2	47.88026	
Temperature	$^{\circ}R$	5/9	kelvin (K)

*Multiply value in U.S. Customary Unit by conversion factor to obtain equivalent value in SI Unit.

**Prefixes to indicate multiples of units are as follows:

Prefix	Multiple
mega (M)	10^6
kilo (k)	10^3
centi (c)	10^{-2}
micro (μ)	10^{-6}

REFERENCES

1. Weinstein, Irving: Heat Transfer and Pressure Distributions on a Hemisphere-Cylinder and a Bluff-Afterbody Model in Methane-Air Combustion Products and in Air. NASA TN D-1503, 1962.
2. Committee on Metric Pract.: ASTM Metric Practice Guide. NBS Handbook 102, U.S. Dep. Com., Mar. 10, 1967.
3. Schaefer, William T., Jr.: Characteristics of Major Active Wind Tunnels at the Langley Research Center. NASA TM X-1130, 1965.
4. Pirrello, C. J.; Hardin, R. D.; Heckart, M. V.; and Brown, K. R.: An Inventory of Aeronautical Ground Research Facilities. Vol. I – Wind Tunnels. NASA CR-1874, 1971.
5. Leyhe, E. W.; and Howell, R. R.: Calculation Procedure for Thermodynamic, Transport, and Flow Properties of the Combustion Products of a Hydrocarbon Fuel Mixture Burned in Air With Results for Ethylene-Air and Methane-Air Mixtures. NASA TN D-914, 1962.
6. Maslowe, S. A.; and Benson, J. L.: Computer Program for the Design and Analysis of Hypersonic Inlets. Rep. No. 18079 (Contract NAS 2-1460), Lockheed-California Co., Aug. 10, 1964. (Available as NASA CR-77749.)
7. Stallings, Robert L., Jr.; and Howell, Dorothy T.: Experimental Pressure Distributions for a Family of Blunt Bodies at Mach Numbers From 2.49 to 4.63 and Angles of Attack From 0^{o} to 15^{o}. NASA TN D-5392, 1969.
8. Baer, A. L.: Pressure Distributions on a Hemisphere Cylinder at Supersonic and Hypersonic Mach Numbers. AEDC-TN-61-96, U.S. Air Force, Aug. 1961.
9. Clark, E. L.: Hemisphere-Cylinder Pressure Distributions at Supersonic and Hypersonic Mach Numbers. AEDC-TR-66-179, U.S. Air Force, 1966. (Available from DDC as AD 804001.)
10. Fay, J. A.; and Riddell, F. R.: Theory of Stagnation Point Heat Transfer in Dissociated Air. J. Aeronaut. Sci., vol. 25, no. 2, Feb. 1958, pp. 73-85, 121.
11. Cohen, Nathaniel B.: Boundary-Layer Similar Solutions and Correlation Equations for Laminar Heat-Transfer Distribution in Equilibrium Air at Velocities up to 41,100 Feet Per Second. NASA TR R-118, 1961.
12. Love, Eugene S.: A Reexamination of the Use of Simple Concepts for Predicting the Shape and Location of Detached Shock Waves. NACA TN 4170, 1957.

13. Choudhury, P. Roy: Shock-Standoff Distance for Spherical Bodies at High Mach Numbers. J. Aerospace Sci., vol. 29, no. 6, June 1962, p. 745.

14. Stollery, J. L.; and Maull, D. J.: A Note on Shock Detachment Distance. J. Roy. Aeronaut. Soc., vol. 64, no. 594, June 1960, pp. 357-359.

TABLE I.- TEST CONDITIONS AND EXPERIMENTAL RESULTS

FOR HEMISPHERE-CYLINDER MODELS

Run	α, deg	M_∞	T_t		R	q_∞		p_s		$\dot{q}_s$	
			K	°R		kN/m^2	lb/ft^2	kN/m^2	psia	MW/m^2	Btu/ft^2-sec
						Model A					
1	0	7.06	1933	3480	0.55×10^6	24.7	516	46.47	6.74	0.369	32.52
2	0	7.36	2056	3700	.38	17.9	373	33.09	4.80	.358	31.56
3	0	6.22	1461	2630	.68	22.4	467	43.09	6.25	.255	22.50
4	0	6.15	1400	2520	.51	15.6	326	29.92	4.34	.193	16.98
5	0	6.95	1922	3460	.84	37.4	782	69.98	10.15	.479	42.20
6	0	6.17	1456	2620	1.01	33.1	691	63.64	9.23	.309	27.24
7	0	7.31	1972	3550	.37	16.1	337	29.51	4.28	.316	27.81
8	0	7.13	1961	3530	.53	23.7	496	44.40	6.44	.382	33.62
9	0	6.85	1900	3420	1.13	50.8	1062	94.67	13.73	.567	50.00
10	0	6.14	1472	2650	1.38	46.3	966	88.80	12.88	.386	34.00
11	0	6.90	1833	3300	.56	23.3	486	43.99	6.38	.356	31.37
						Model B					
12	-0.2	6.82	1778	3200	1.26×10^6	25.5	532	48.26	7.00	----	----
12	17.8	6.82	1778	3200	1.26	25.5	532	48.26	7.00	----	----
13	-.3	6.78	1756	3160	1.22	24.7	515	46.75	6.78	----	----
↓	11.1	↓	↓	↓	↓	↓	↓	↓	↓	----	----
↓	13.0	↓	↓	↓	↓	↓	↓	↓	↓	----	----
↓	14.9	↓	↓	↓	↓	↓	↓	↓	↓	----	----
↓	16.9	↓	↓	↓	↓	↓	↓	↓	↓	----	----
						Model C					
14	0	7.07	1922	3460	0.63×10^6	23.3	487	*43.71	6.34	0.404	35.60
15	0	6.42	1644	2960	1.34	43.7	913	*83.57	12.12	.418	36.83

*Values determined theoretically.

TABLE II.- PRESSURE DISTRIBUTIONS p/p_s ON MODEL A

θ, deg	β, deg	$\bar{s}/r$	p/p_s for run –										
			1	2	3	4	5	6	7	8	9	10	11
*5	75	0.087											
10	285	.175	0.972	0.976	0.970	0.970	0.963	0.966	0.973	0.970	0.964	0.965	0.969
20	135	.349	.851	.837	.865	.848	.858	.866	.843	.847	.867	.870	.860
30	165	.524	.739	.746	.754	.760	.733	.748	.752	.738	.730	.742	.751
40	195	.698	.574	.579	.584	.588	.566	.586	.586	.572	.565	.578	.581
45	225	.785	.484	.480	.493	.490	.477	.492	.488	.482	.489	.494	.491
50	255	.873	.399	.396	.398	.391	.395	.404	.385	.392	.399	.404	.394
60	105	1.047	.270	.269	.270	.269	.266	.268	.270	.270	.288	.269	.272
60	285	1.047	.260	.258	.257	.254	.286	.293	.273	.277	.295	.303	.303
70	315	1.222	.1632	.1636	.1636	.1621	.1620	.1620	.1648	.1638	.1894	.1628	.1655
80	345	1.396	.0953	.0973	.0951	.0952	.0936	.0922	.0979	.0959	.1028	.0919	.0973
85	15	1.484	.0715	.0504	.0566	.0708	-----	-----	-----	-----	-----	-----	-----
90	45	1.571	.0526	.0555	.0508	.0516	.0520	.0489	.0558	.0534	.0513	.0487	.0545
	225	1.738	.0481	.0510	.0455	.0465	.0483	.0453	.0505	.0490	.0482	.0450	.0494
	75	2.071	.0380	.0461	.0420	.0428	.0445	.0406	.0459	.0448	.0447	.0406	.0457
	285	2.238	.0352	.0443	.0414	.0420	.0434	.0408	.0441	.0439	.0434	.0405	.0444
	135	2.571	-----	.0409	.0380	.0386	.0403	.0369	.0407	.0400	.0406	.0370	.0413
	45	2.904	.0380	.0400	.0358	.0372	.0378	.0350	.0396	.0384	.0378	.0346	.0392
	225	2.904	-----	.0408	.0380	.0385	.0403	.0366	.0410	.0405	.0404	.0366	.0412
	195	3.571	.0333	.0362	.0326	.0341	.0340	.0314	.0358	.0346	.0338	.0309	.0356
	165	4.238	.0301	.0320	.0292	.0309	.0303	.0280	.0320	.0308	.0302	.0275	.0318
	315	4.738	.0301	.0319	.0286	.0303	.0292	.0271	.0317	.0303	.0293	.0265	.0311
	90	5.071	.0289	.0312	.0275	.0293	.0281	.0260	.0309	.0292	.0280	.0254	.0302
	270	5.571	.0276	.0302	.0263	.0282	.0268	.0248	.0299	.0280	.0265	.0241	.0289

* 5° location used to obtain Newtonian stagnation values which were then used to nondimensionalize all pressures.

TABLE III.- HEATING DISTRIBUTIONS $\dot{q}/\dot{q}_S$ ON MODEL A

θ, deg	β, deg	$\bar{s}/r$	$\dot{q}/\dot{q}_S$ for run –										
			1	2	3	4	5	6	7	8	9	10	11
0	0	0	1.000	1.000	1.000	1.000	1.000	1.000	1.000	1.000	1.000	1.000	1.000
5	0	.087	.981	.985	.982	.981	.977	.964	.983	.984	.972	.957	.982
10	0	.175	.960	.972	.954	.966	.960	.943	.973	.973	.953	.930	.965
10	180	.175	.951	.957	.942	.906	.945	.931	.968	.958	.993	.925	.966
20	0	.349	.889	.898	.881	.885	.891	.861	.902	.900	.883	.850	.890
30	0	.524	.775	.784	.700	.781	.780	.753	.786	.785	.773	.742	.780
40	0	.698	.637	.637	.630	.639	.647	.618	.643	.644	.637	.608	.638
40	90	.698	.637	.634	.626	.639	.639	.591	.638	.644	.632	.608	.635
40	180	.698	.610	.616	.609	.621	.615	.600	.619	.613	.593	.592	.544
40	270	.698	.625	.625	.623	.623	.645	.613	.607	.632	.634	.605	.639
45	0	.785	.566	.572	.565	.567	.572	.550	.567	.568	.569	.535	.562
50	0	.873	.496	.494	.494	.491	.500	.477	.496	.499	.499	.471	.497
60	0	1.047	.354	.348	.354	.342	.354	.338	.355	.357	.355	.332	.354
70	0	1.222	.247	.233	.242	.239	.242	.229	.240	.244	.241	.231	.242
80	0	1.396	.1545	.1456	.1559	.1721	.1522	.1494	.1545	.1552	.1564	.1471	.1553
80	180	1.396	.1442	.1390	.1399	.1320	.1498	.1360	.1475	.1598	.1492	.1346	.1459
85	0	1.484	.1182	.1159	.1191	.1205	.1218	.1140	.1189	.1206	.1232	.1146	.1196
90	0	1.571	.0898	.0871	.0879	.0881	.0903	.0828	.0971	.0932	.0928	.0865	.0892
	0	1.738	.0757	.0684	.0710	.0645	.0768	.0692	.0746	.0751	.0763	.0687	.0737
	0	2.029	.0691	.0603	.0622	.0625	.0680	.0593	.0667	.0674	.0685	.0617	.0661
	0	2.238	.0621	.0580	.0606	.0554	.0629	.0528	.0613	.0623	.0633	.0566	.0606
	180	2.238	.0526	.0591	.0542	.0557	.0596	.0493	.0546	.0585	.0552	.0534	.0579
	0	2.571	.0538	.0520	.0509	.0488	.0560	.0483	.0543	.0551	.0560	.0516	.0551
	0	2.904	.0506	.0463	.0482	.0440	.0497	.0434	.0460	.0502	.0496	.0461	.0461
	0	3.238	.0434	.0405	.0439	.0412	.0457	.0416	.0460	.0473	.0440	.0425	.0469
	0	3.571	.0401	.0393	.0403	.0407	.0418	.0376	.0429	.0418	.0425	.0392	.0418
	0	3.904	.0385	.0378	.0360	.0351	.0395	.0368	.0369	.0397	.0386	.0399	.0410
	180	3.904	.0362	.0375	.0350	.0348	.0414	.0352	.0380	.0373	.0374	.0347	.0392
	0	4.571	.0344	.0346	.0354	.0341	.0337	.0319	.0338	.0351	.0352	.0330	.0384
	0	5.071	.0341	.0297	.0314	.0316	.0317	.0322	.0324	.0319	.0324	.0338	.0342
	0	5.571	.0288	.0282	.0314	-----	.0318	-----	.0298	.0290	.0302	.0350	.0303

TABLE IV.- HEATING DISTRIBUTIONS $\dot{q}/\dot{q}_s$ ON MODEL C

θ, deg	β, deg	$\bar{s}/r$	$\dot{q}/\dot{q}_s$ for run –	
			14	15
0	0	0	1.000	1.000
5	0	.087	.990	.950
10	0	.175	.961	.888
10	180	.175	.907	.848
20	0	.349	.885	.826
30	0	.524	.740	.720
30	180	.524	.871	.807
40	0	.698	.564	.557
50	0	.873	.475	.472
60	0	1.047	.356	.345
60	90	1.047	.362	.357
60	180	1.047	.368	.353
60	270	1.047	.377	.367
70	0	1.222	.246	.237
80	0	1.396	.1343	.1398
85	0	1.484	.0888	.0881
90	180	1.571	.0938	.0889
	0	1.713	.0837	.0799
	180	1.713	.0916	.0874
	0	1.855	.0740	.0721
	0	2.140	.0679	.0687
	180	2.140	.0673	.0686
	0	2.424	.0563	.0611
	0	2.709	.0590	.0575
	180	2.709	.0690	.0698
	0	3.278	.0499	.0521

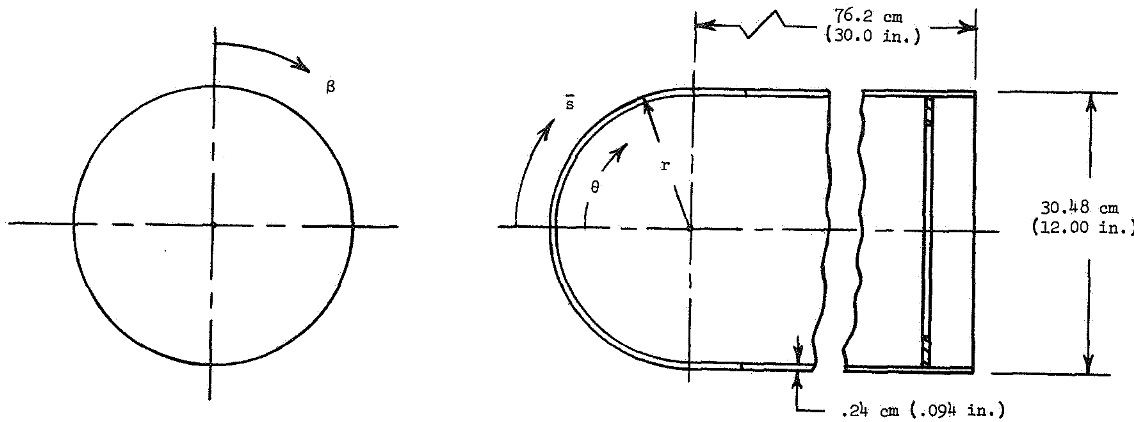

Pressure orifice locations		
$\bar{s}/r$	θ, deg	β, deg
0.087	5	75
.175	10	285
.349	20	135
.524	30	165
.698	40	195
.785	45	225
.873	50	255
1.047	60	105
1.047	60	285
1.222	70	315
1.396	80	345
1.484	85	15
1.571	90	45
1.738		225
2.071		75
2.238		285
2.571		135
2.904		45
2.904		225
3.571		195
4.238		165
4.738		315
5.071		90
5.571		270

Thermocouple locations					
$\bar{s}/r$	θ, deg	β, deg	$\bar{s}/r$	θ, deg	β, deg
0	0	0	1.484	85	0
.087	5	0	1.571	90	0
.175	10	0	1.738		0
.175	10	180	2.029		0
.349	20	0	2.238		0
.524	30	0	2.238		180
.698	40	0	2.571		0
.698	40	90	2.904		0
.698	40	180	3.238		0
.698	40	270	3.571		0
.785	45	0	3.904		0
.873	50	0	3.904		180
1.047	60	0	4.571		0
1.222	70	0	5.071		0
1.396	80	0	5.571		0
1.396	80	180			

(a) Pressure orifice and thermocouple locations for model A.

Figure 1.- Instrumentation location and photograph of model A.

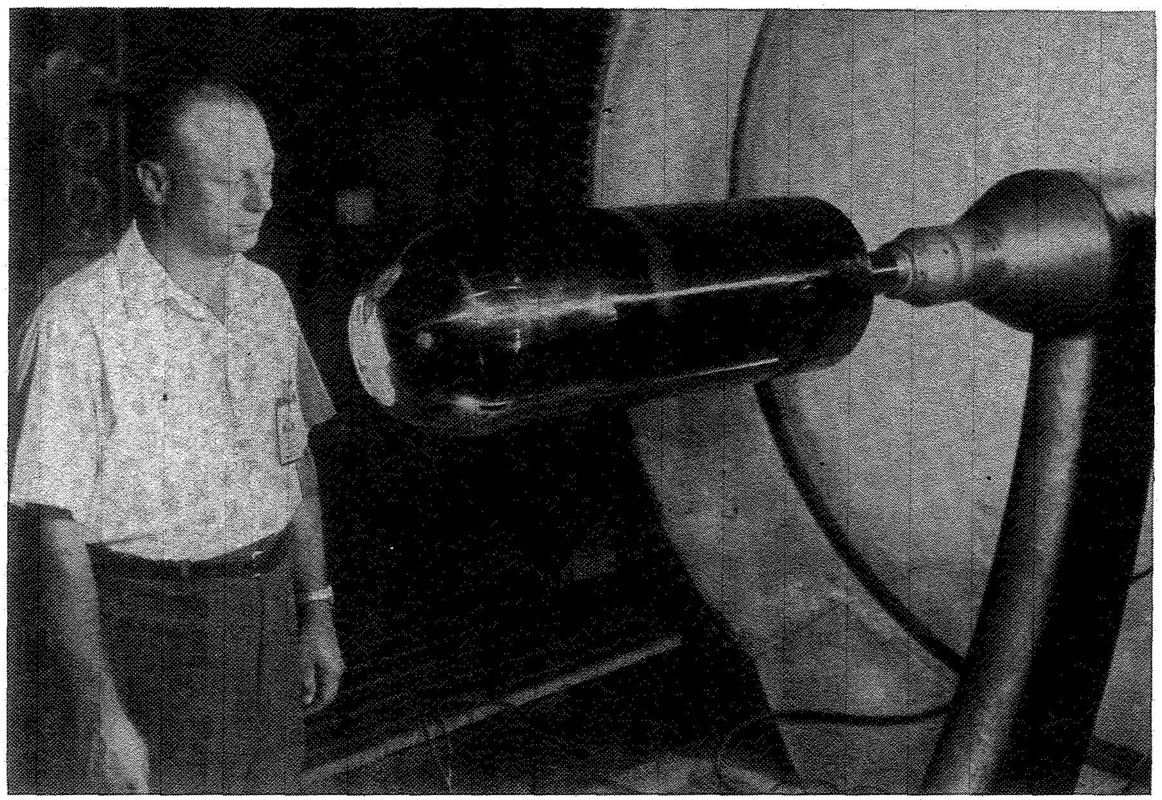

L-72-6585

(b) Photograph of model A in Langley 8-foot high-temperature structures tunnel.

Figure 1.- Concluded.

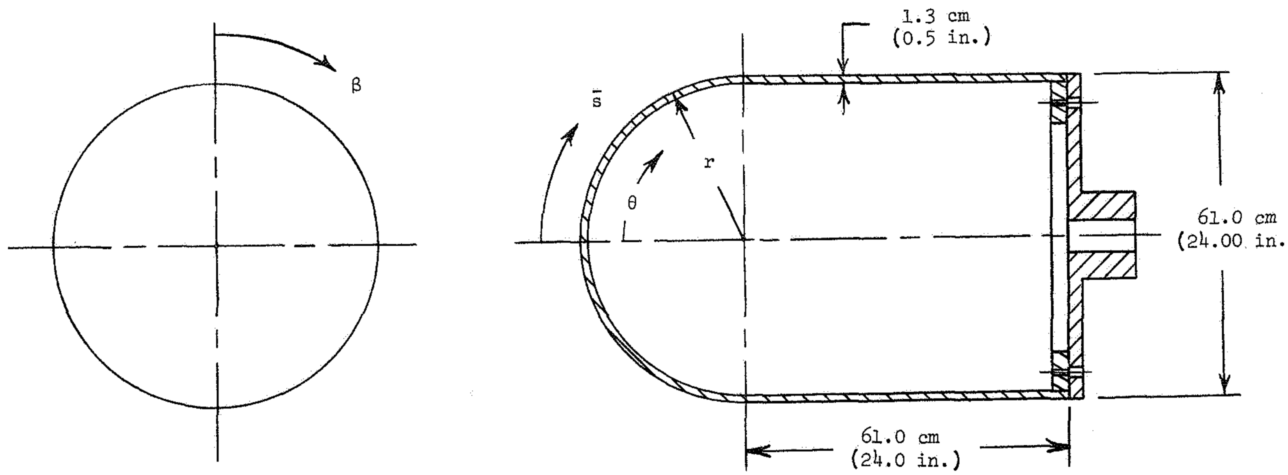

Pressure orifice locations		
$\bar{s}/r$	θ, deg	β,deg
0	0	0
.524	30	0
.524	30	90
.524	30	180
.524	30	270
1.047	60	0
1.047	60	180
2.071		0
2.071		180
3.071		0
3.071		180

(a) Sketch and pressure orifice locations for model B.

Figure 2.- Pressure orifice locations and photograph of model B.

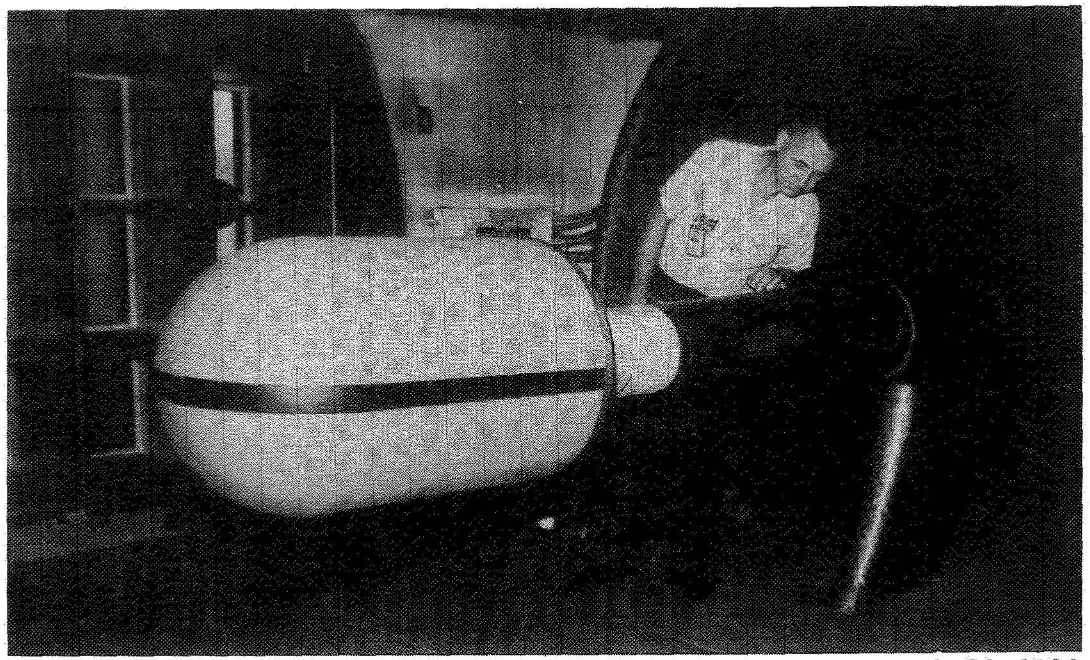

L-72-6586

(b) Photograph of model B in Langley 8-foot high-temperature structures tunnel.

Figure 2.- Concluded.

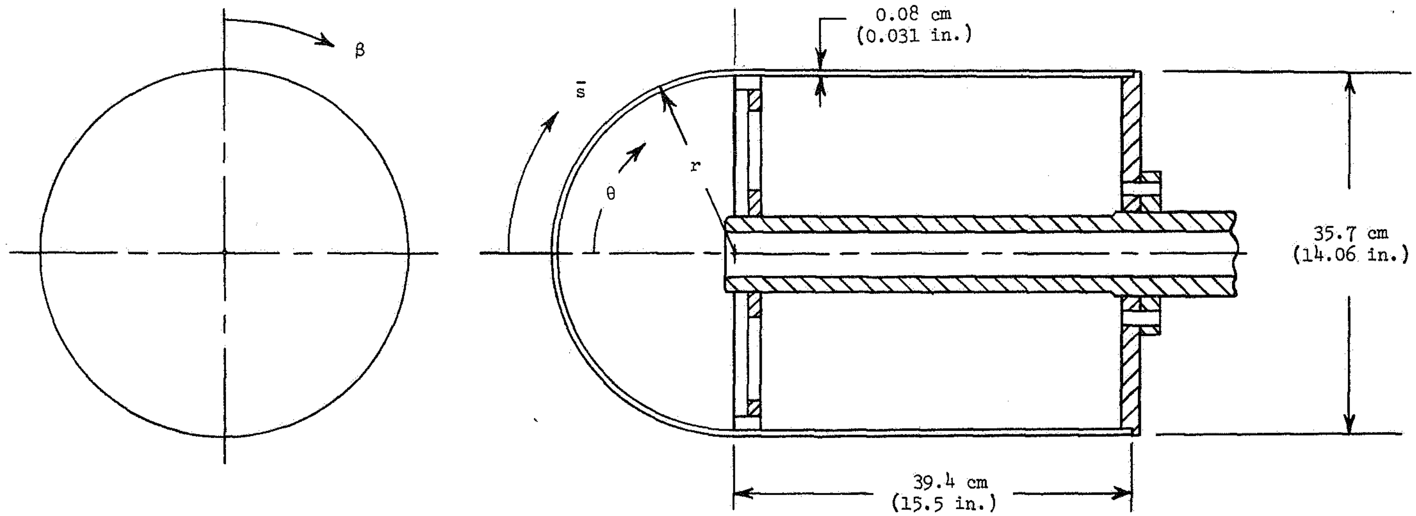

Thermocouple locations					
$\bar{s}/r$	θ, deg	β, deg	$\bar{s}/r$	θ, deg	β, deg
0	0	0	1.222	70	0
.087	5	0	1.396	80	0
.175	10	0	1.484	85	0
.175	10	180	1.571	90	180
.349	20	0	1.713		0
.524	30	0	1.713		180
.524	30	180	1.855		0
.698	40	0	2.140		0
.873	50	0	2.140		180
1.047	60	0	2.424		0
1.047	60	90	2.709		0
1.047	60	180	2.709		180
1.047	60	270	3.278		0

(a) Sketch and thermocouple locations for model C.

Figure 3.- Sketch, table of thermocouple locations, and photograph of model C.

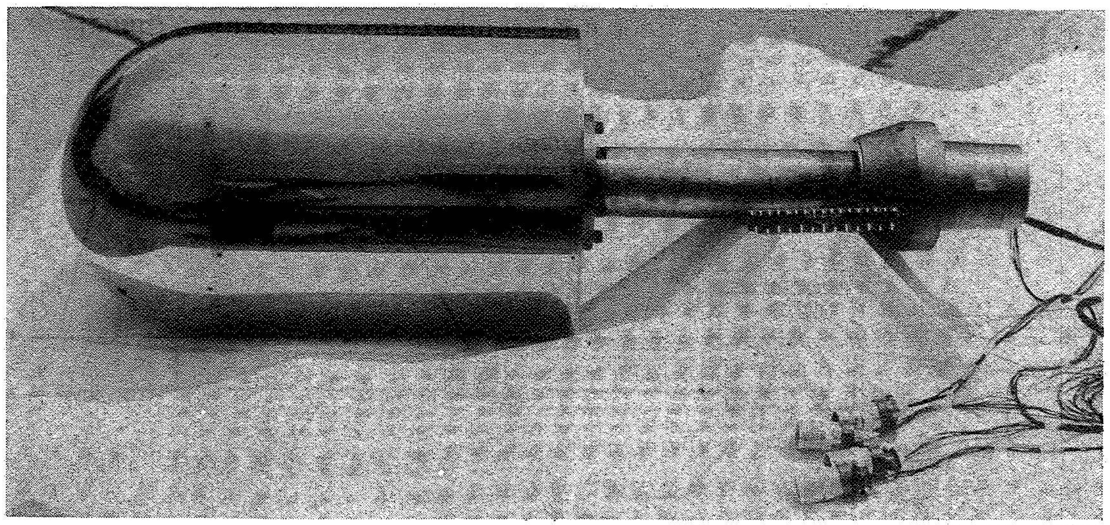

L-72-6587

(b) Photograph of model C.

Figure 3.- Concluded.

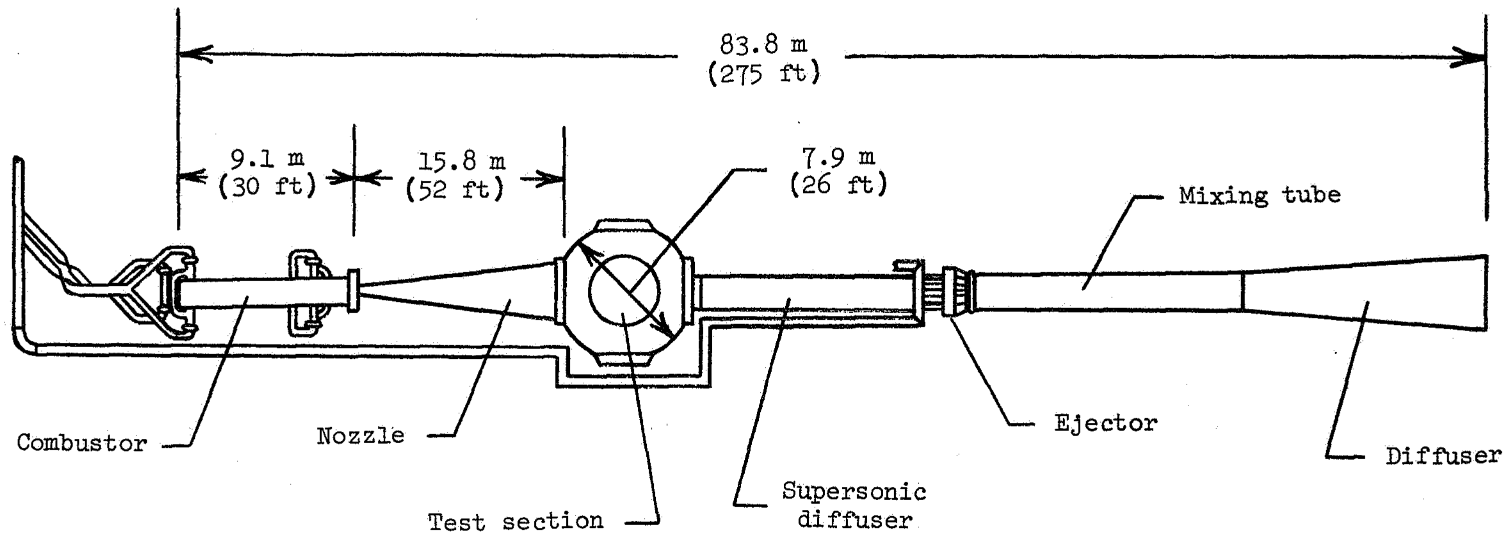

Figure 4.- Schematic of the Langley 8-foot high-temperature structures tunnel.

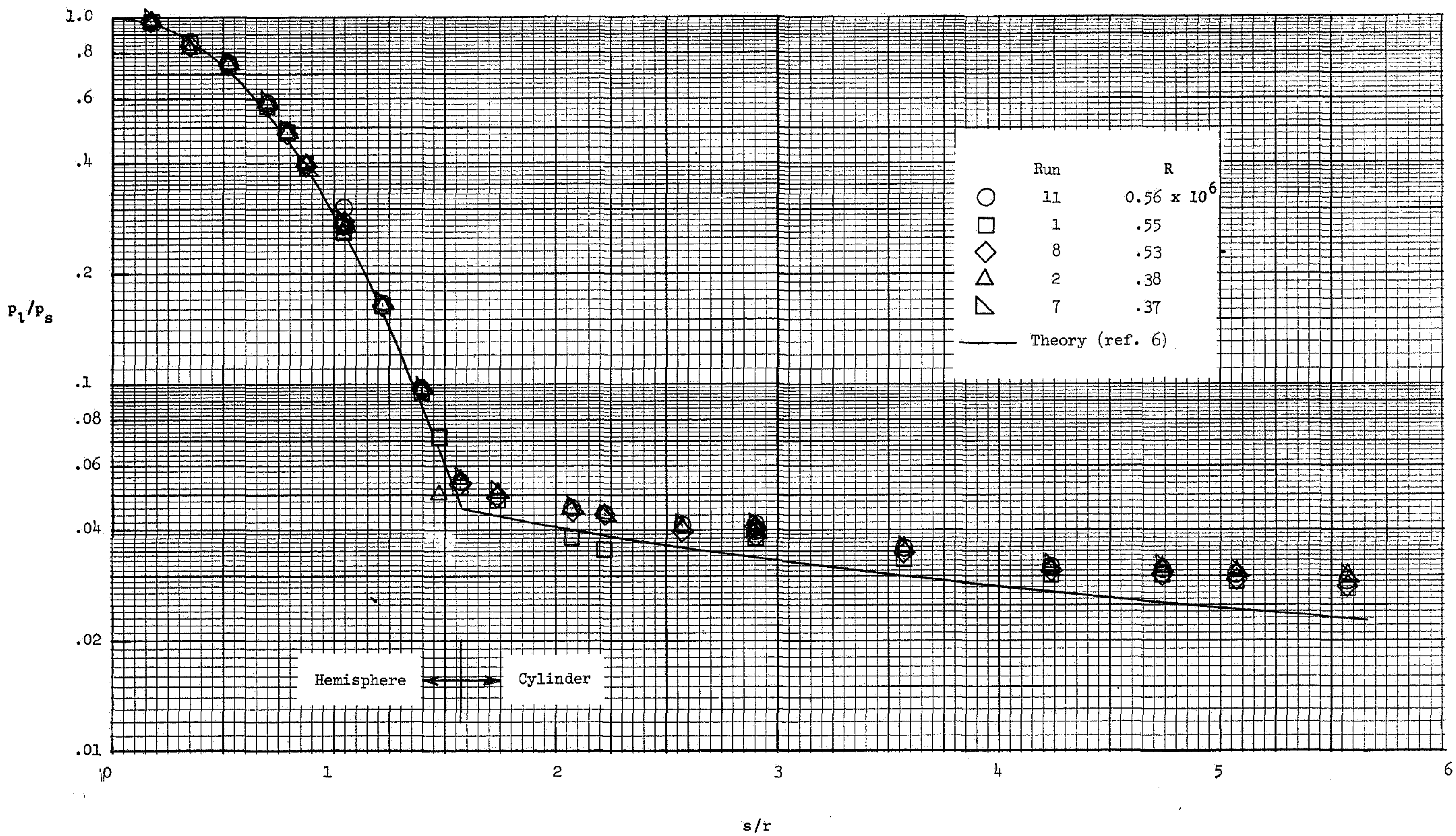

(a) Low-pressure and high-temperature tests.

Figure 5.- Longitudinal nondimensional pressure distributions on model A at $\alpha = 0^{o}$.

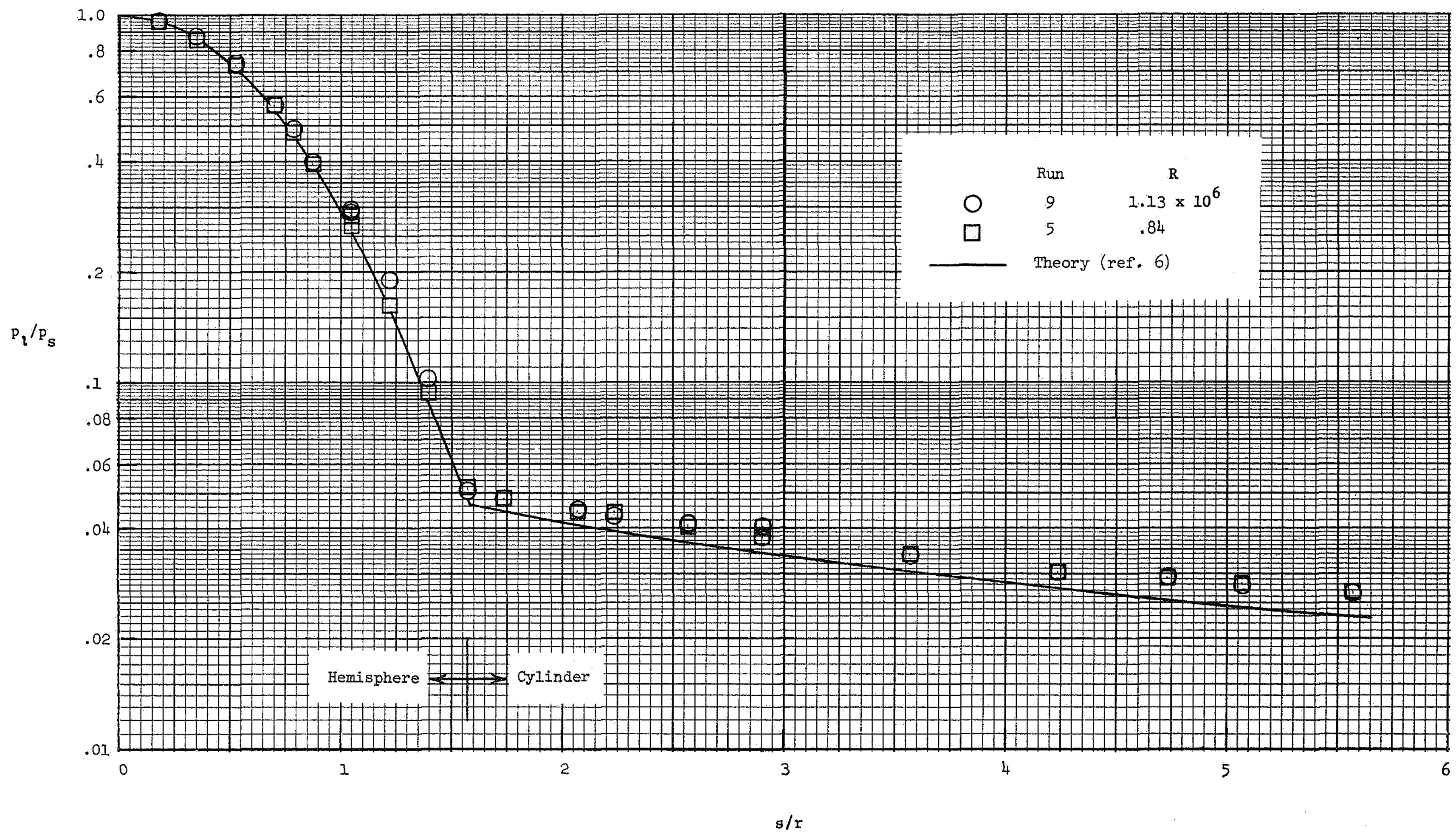

(b) High-pressure and high-temperature tests.

Figure 5.- Continued.

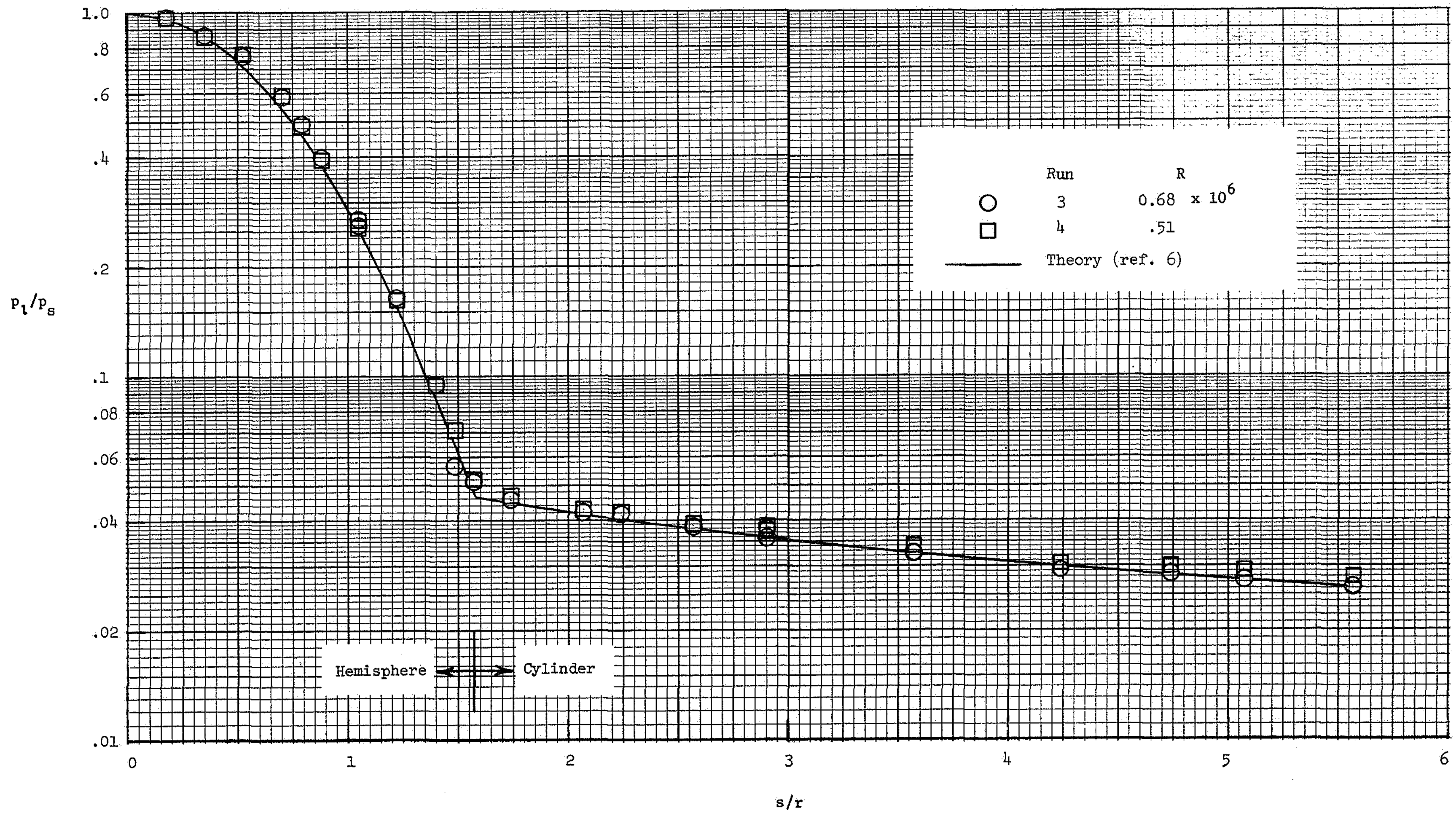

(c) Low-pressure and low-temperature tests.

Figure 5.- Continued.

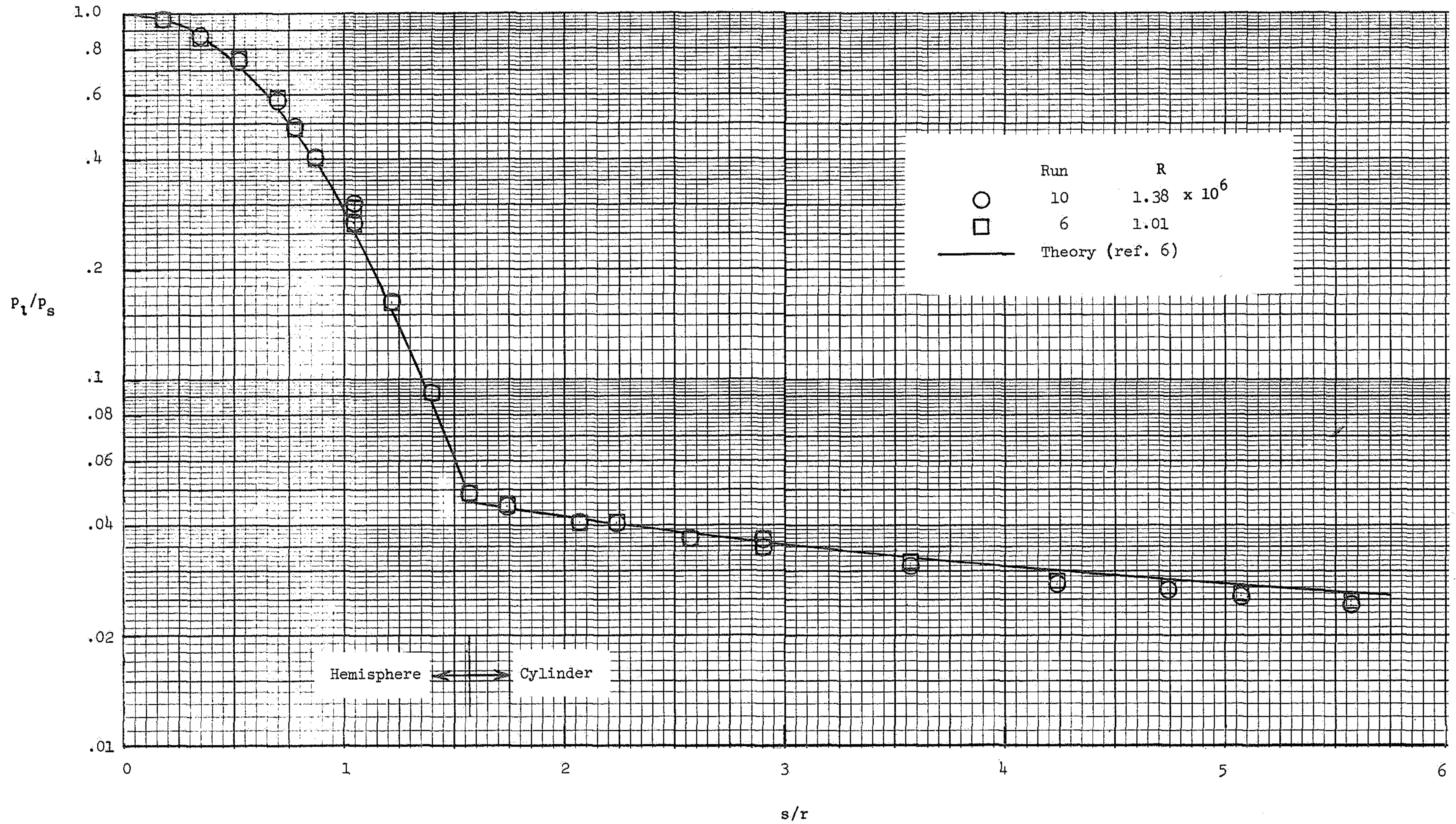

(d) High-pressure and low-temperature tests.

Figure 5.- Concluded.

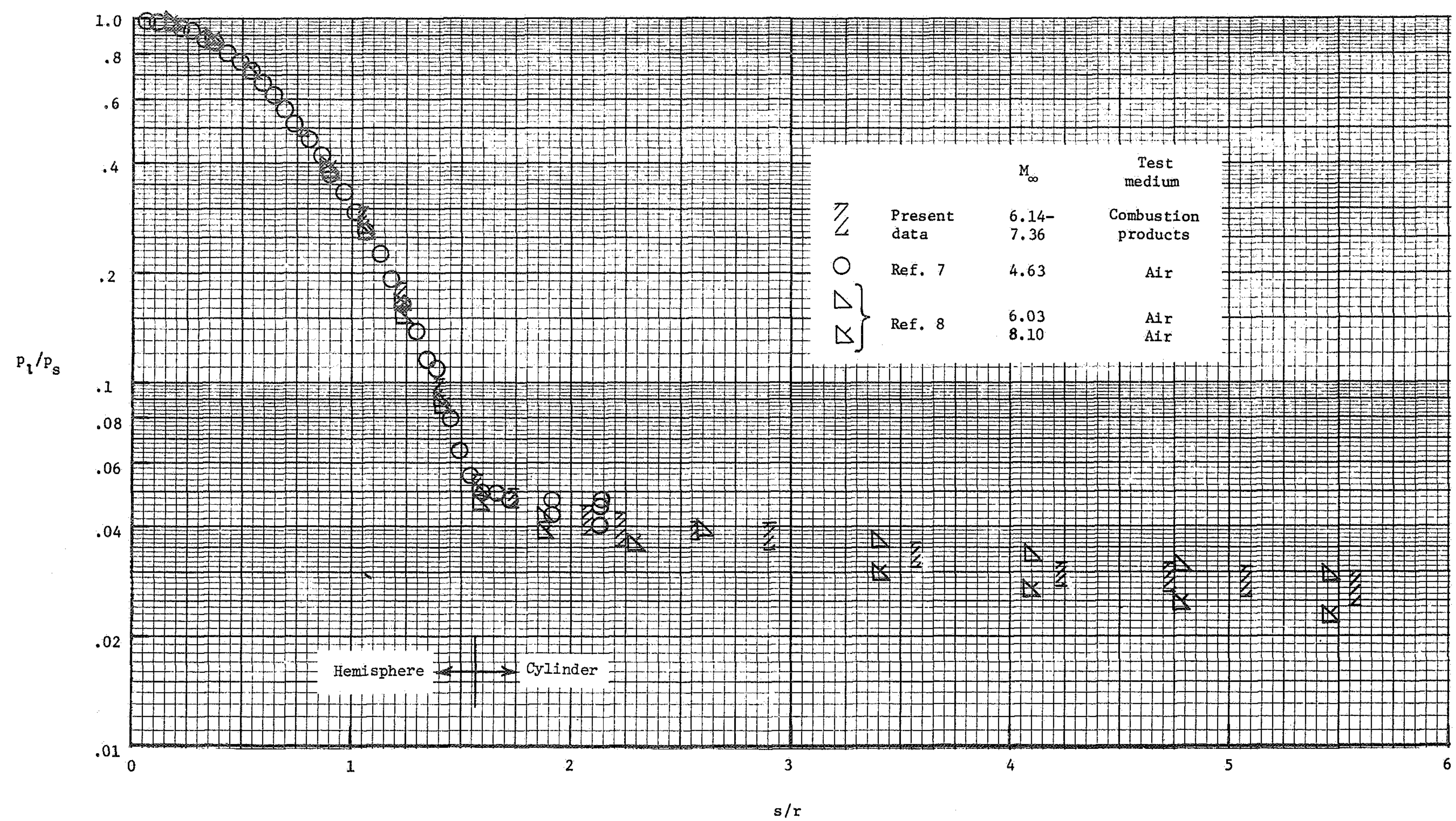

Figure 6.- Comparison of pressure distributions obtained in combustion products and in air.

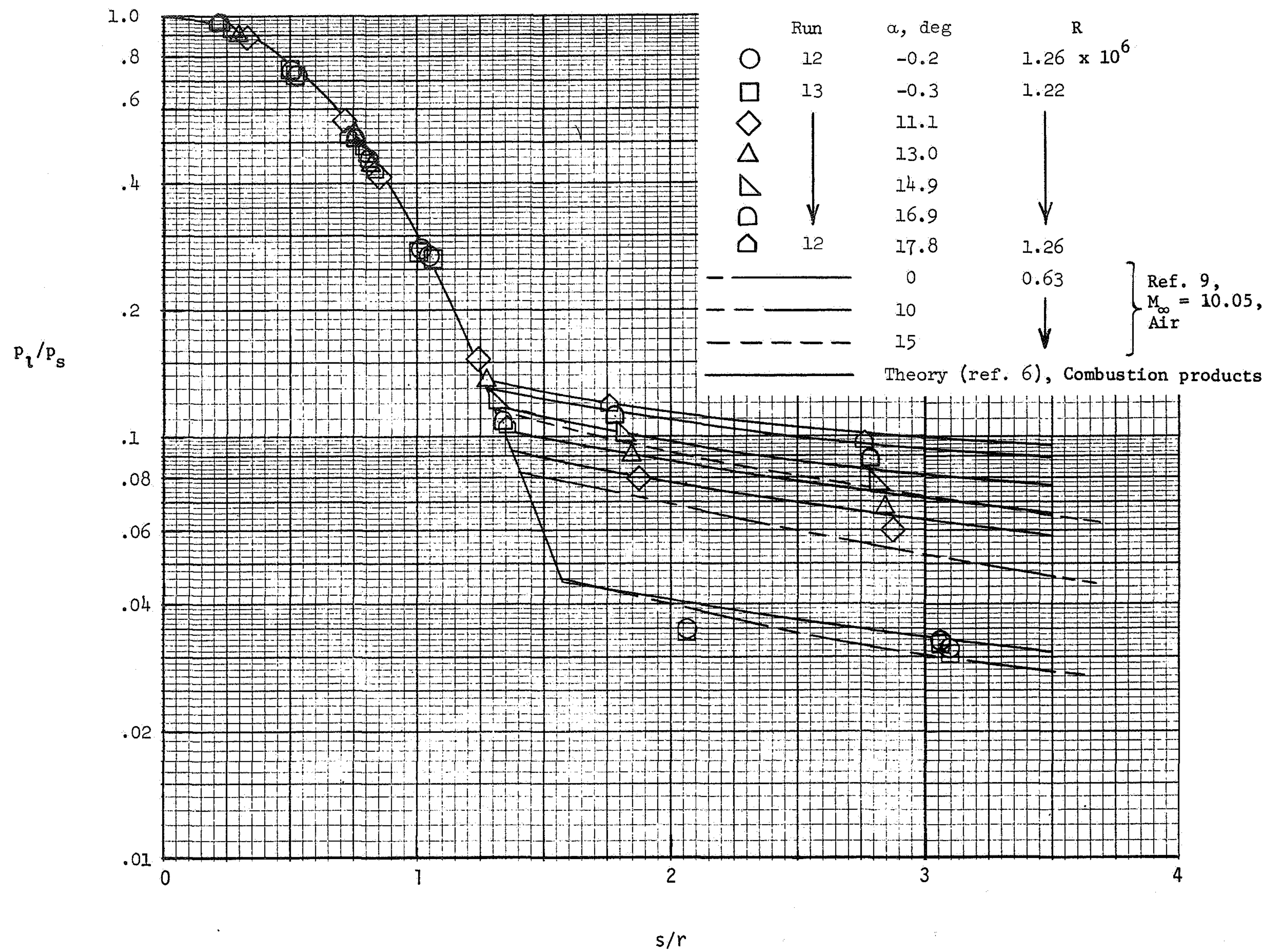

Figure 7.- Longitudinal pressure distributions at angle of attack on model B.

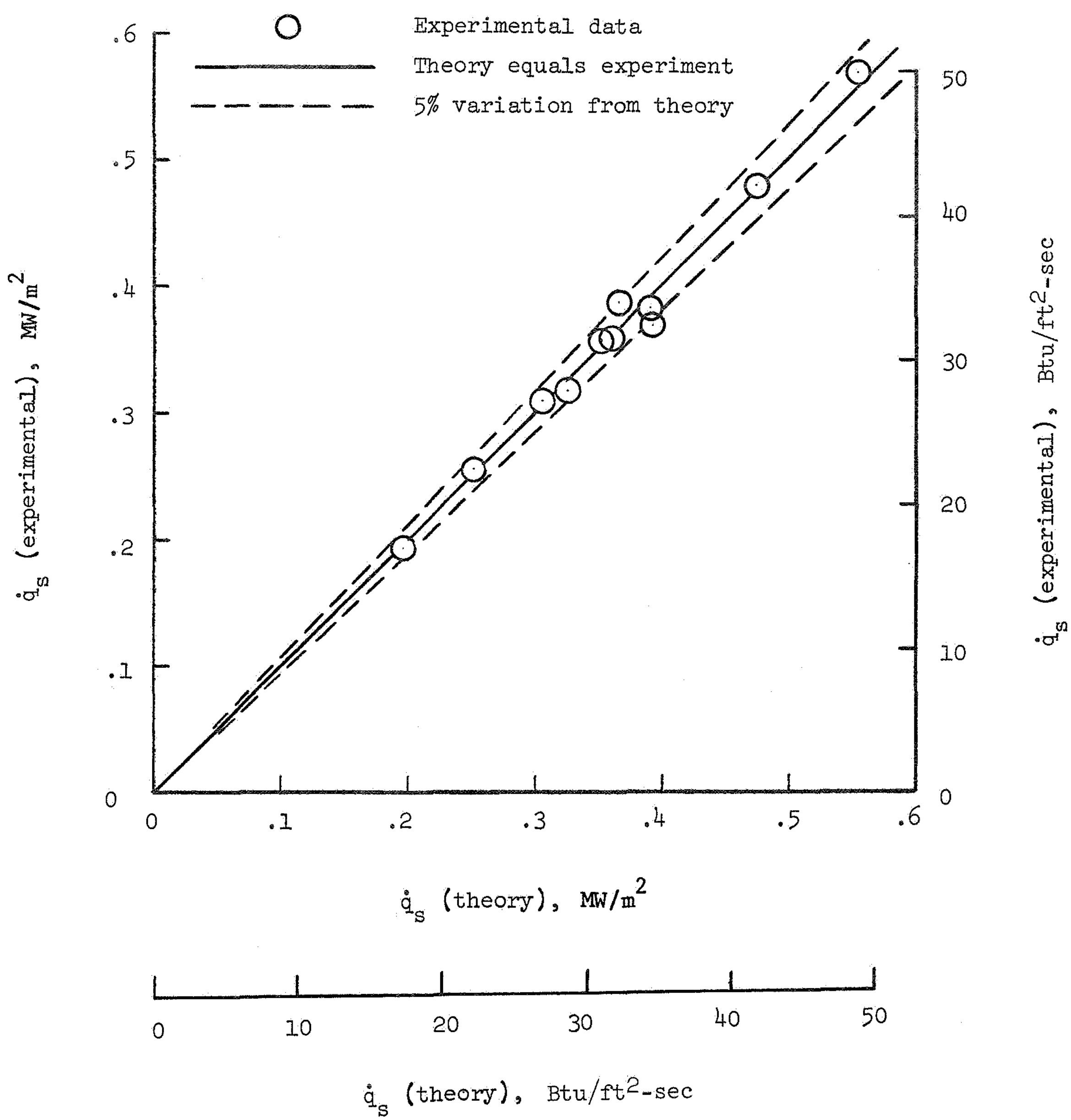

Figure 8.- Comparison of experimental and theoretical stagnation-point heating rates on model A.

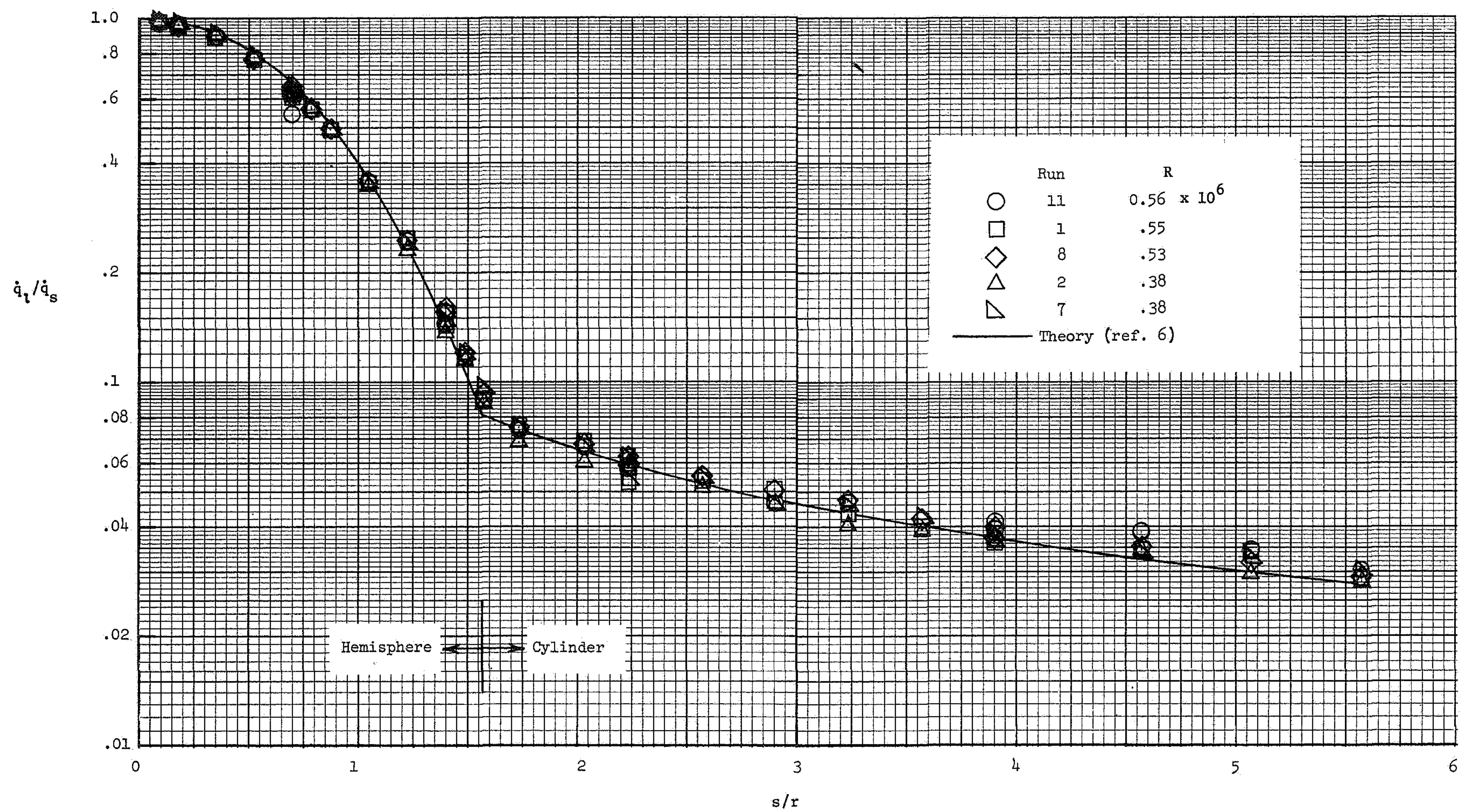

(a) Low-pressure and high-temperature tests.

Figure 9.- Longitudinal nondimensional heating distributions on model A at $\alpha = 0^{\circ}$.

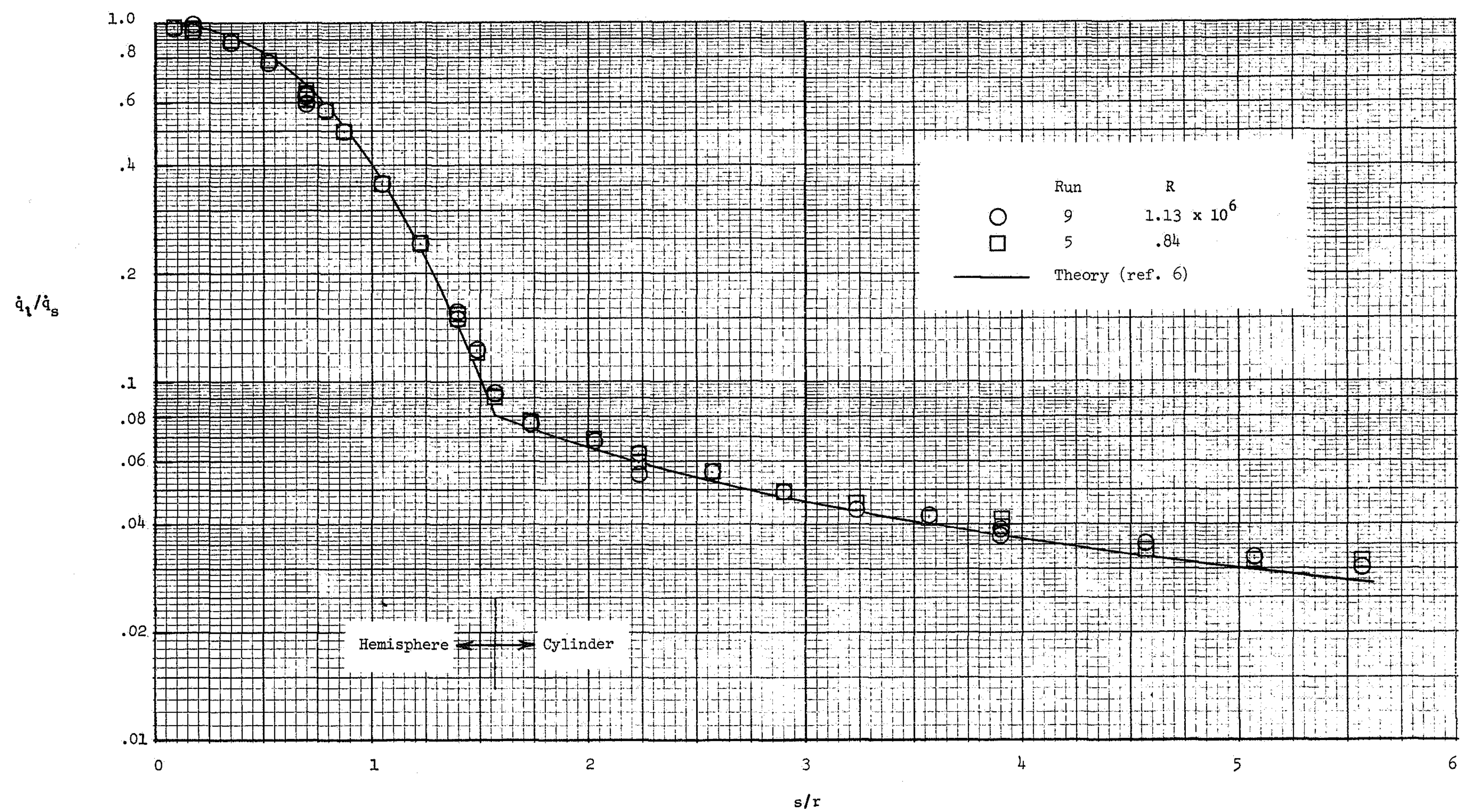

(b) High-pressure and high-temperature tests.

Figure 9.- Continued.

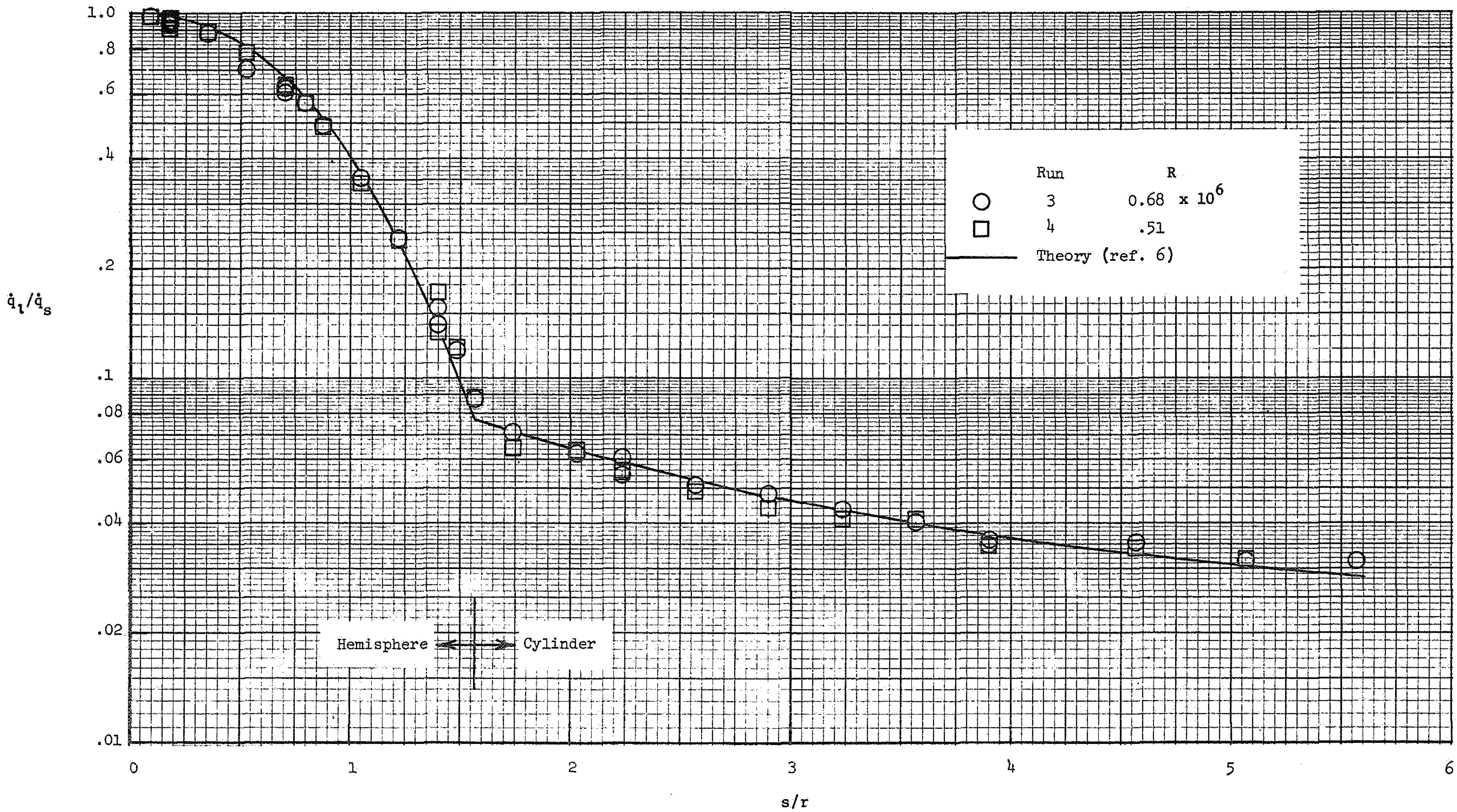

(c) Low-pressure and low-temperature tests.

Figure 9.- Continued.

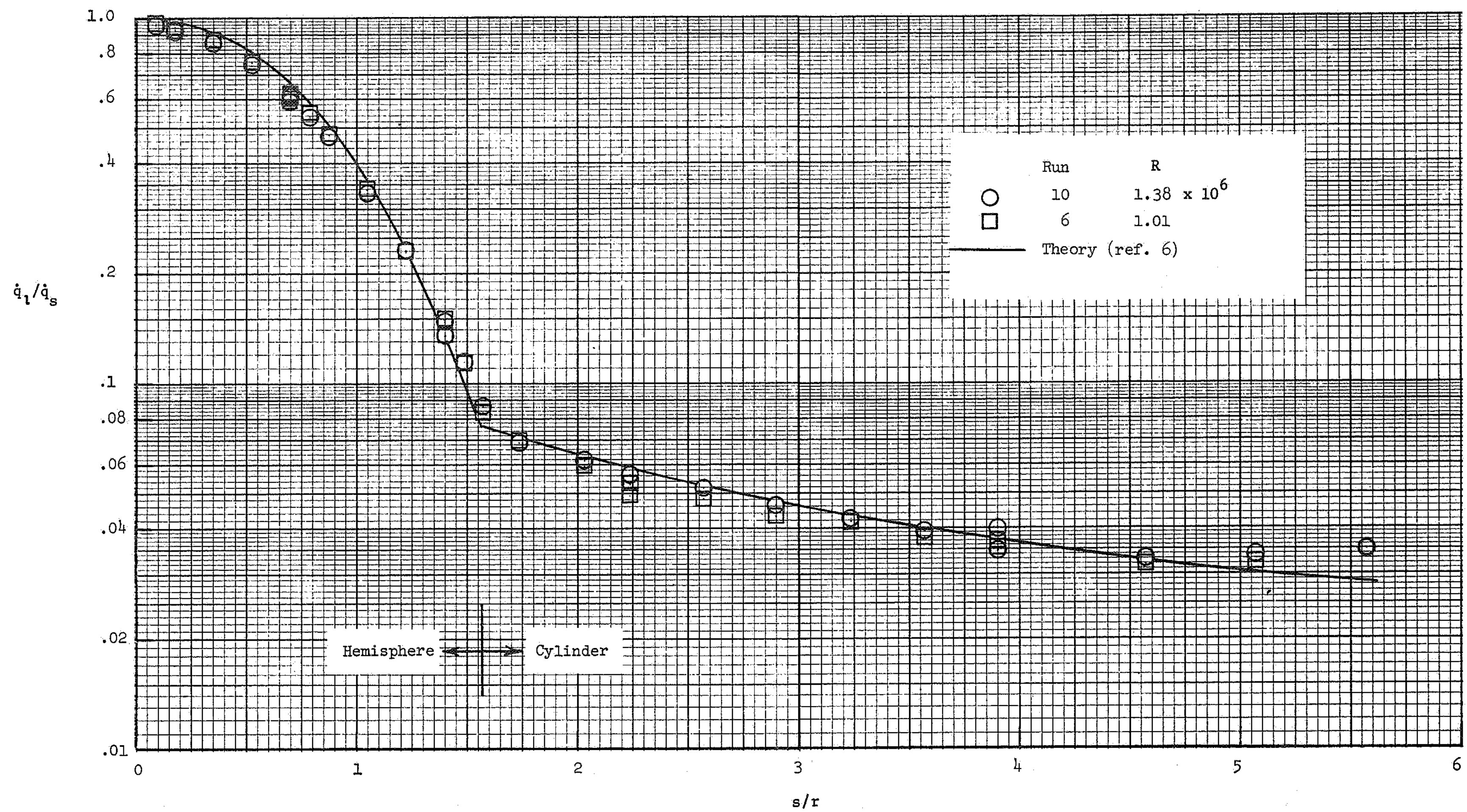

(d) High-pressure and low-temperature tests.

Figure 9.- Concluded.

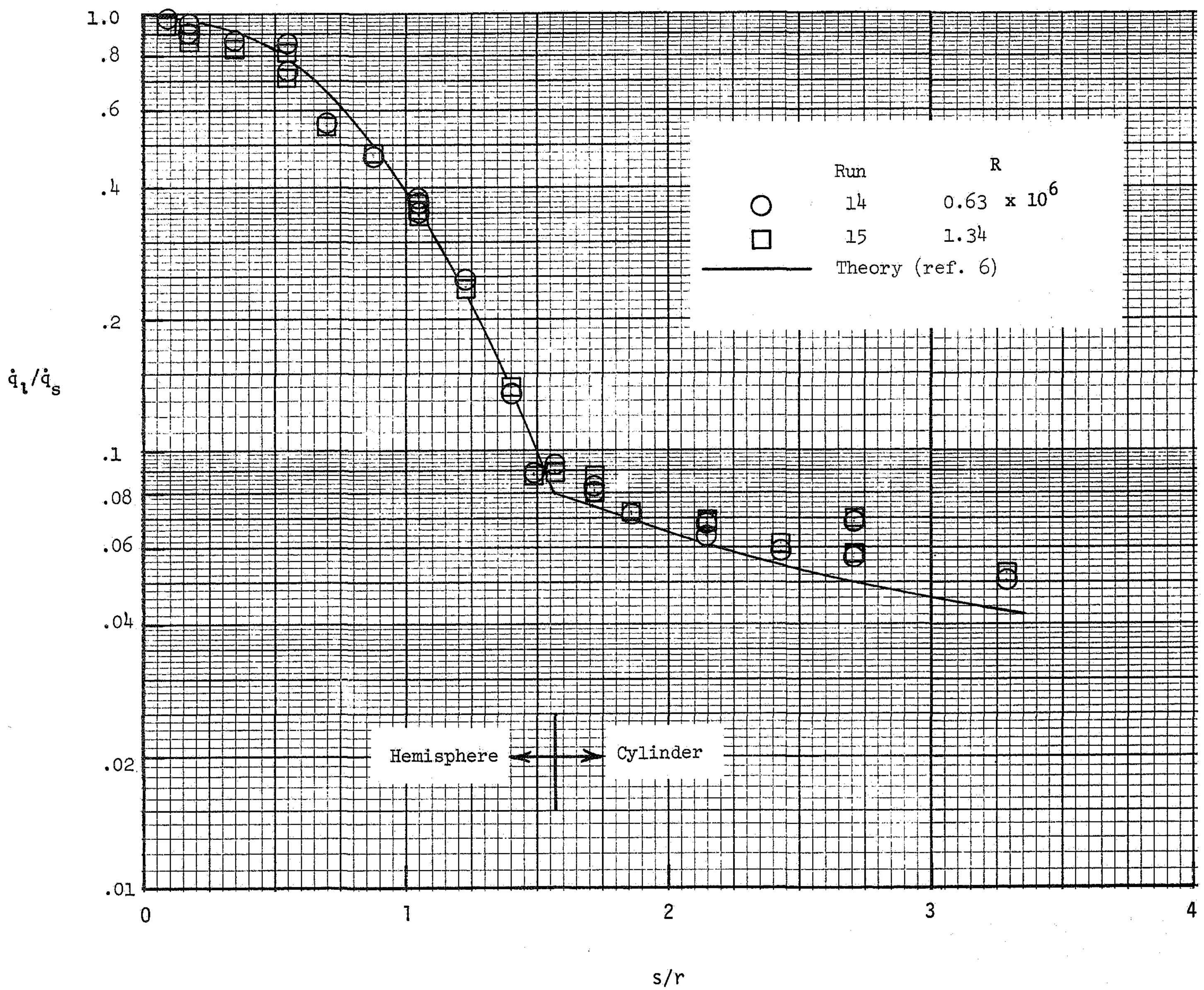

Figure 10.- Longitudinal nondimensional heating distributions on model C at $\alpha = 0^{\circ}$.

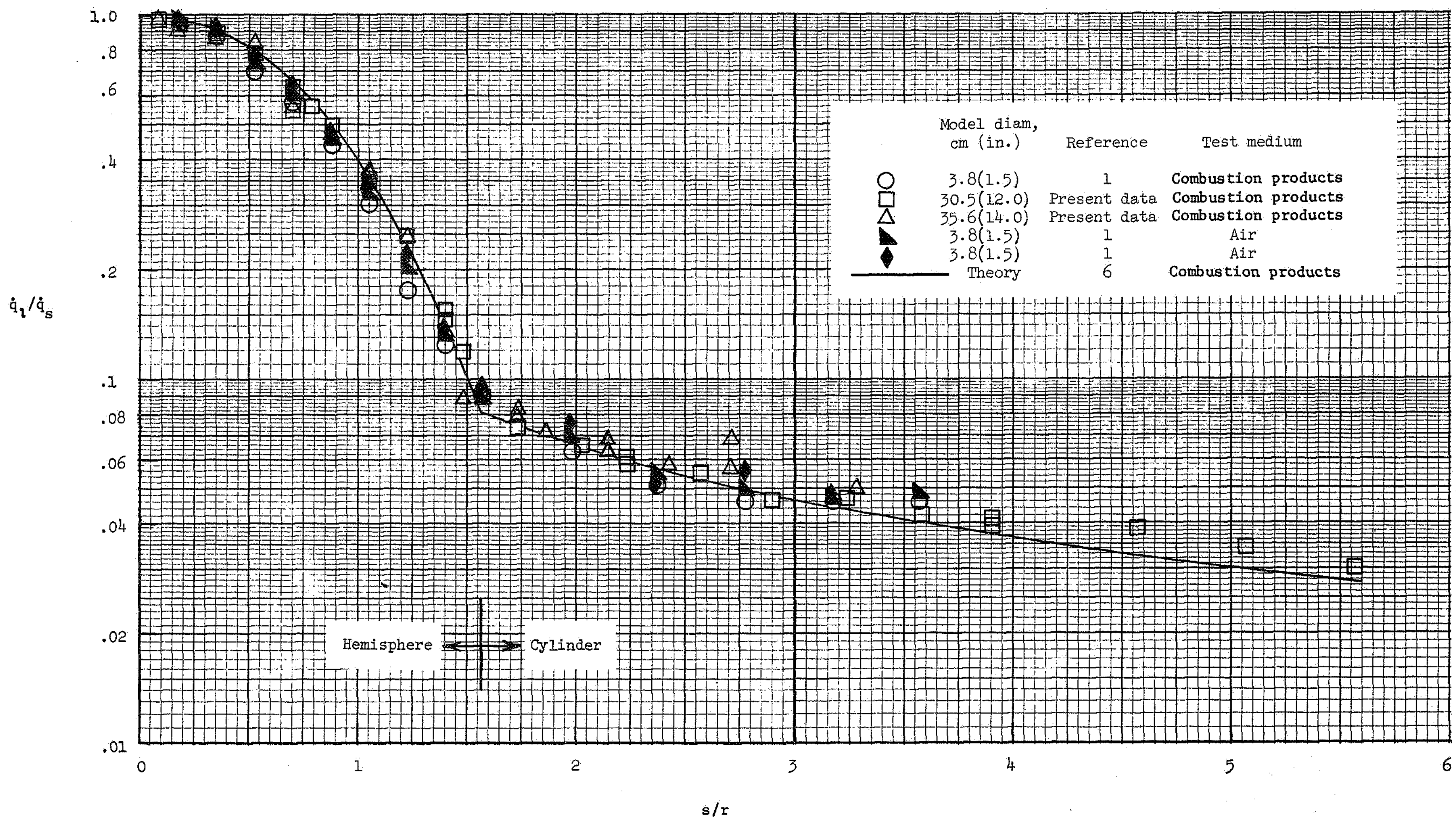

Figure 11.- Correlation of heating distributions obtained in combustion products and in air.

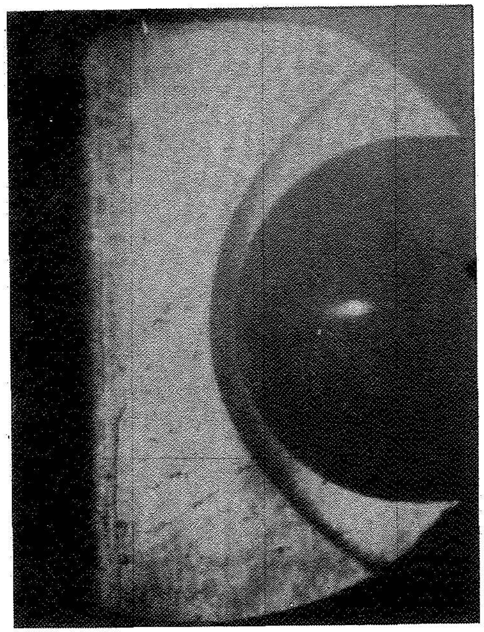

Run 4
$R = 0.51 \times 10^6$

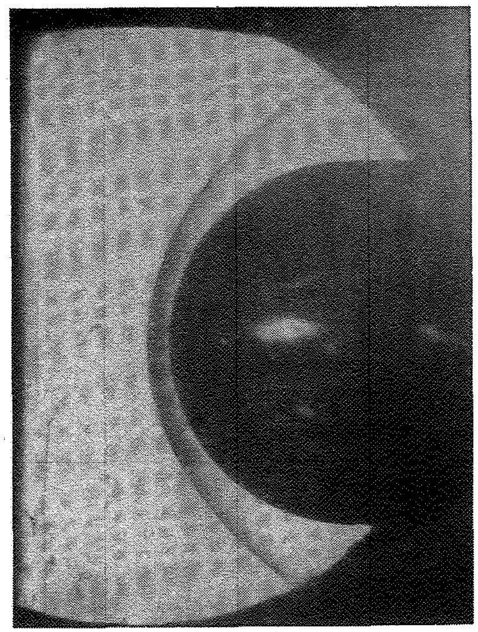

Run 7
$R = 0.37 \times 10^6$

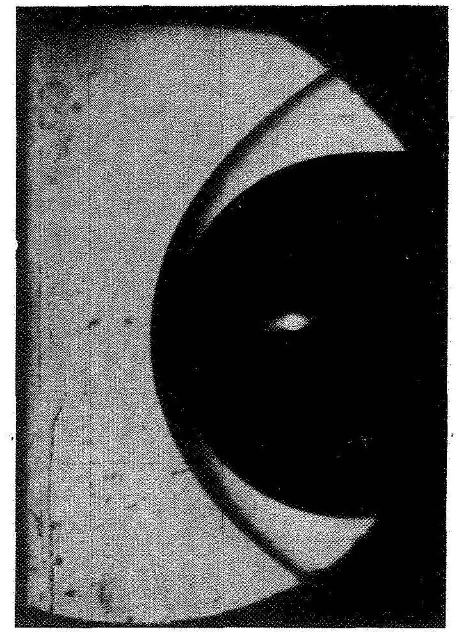

Run 9
$R = 1.13 \times 10^6$

L-72-6588

Figure 12.- Schlieren photographs of model A.

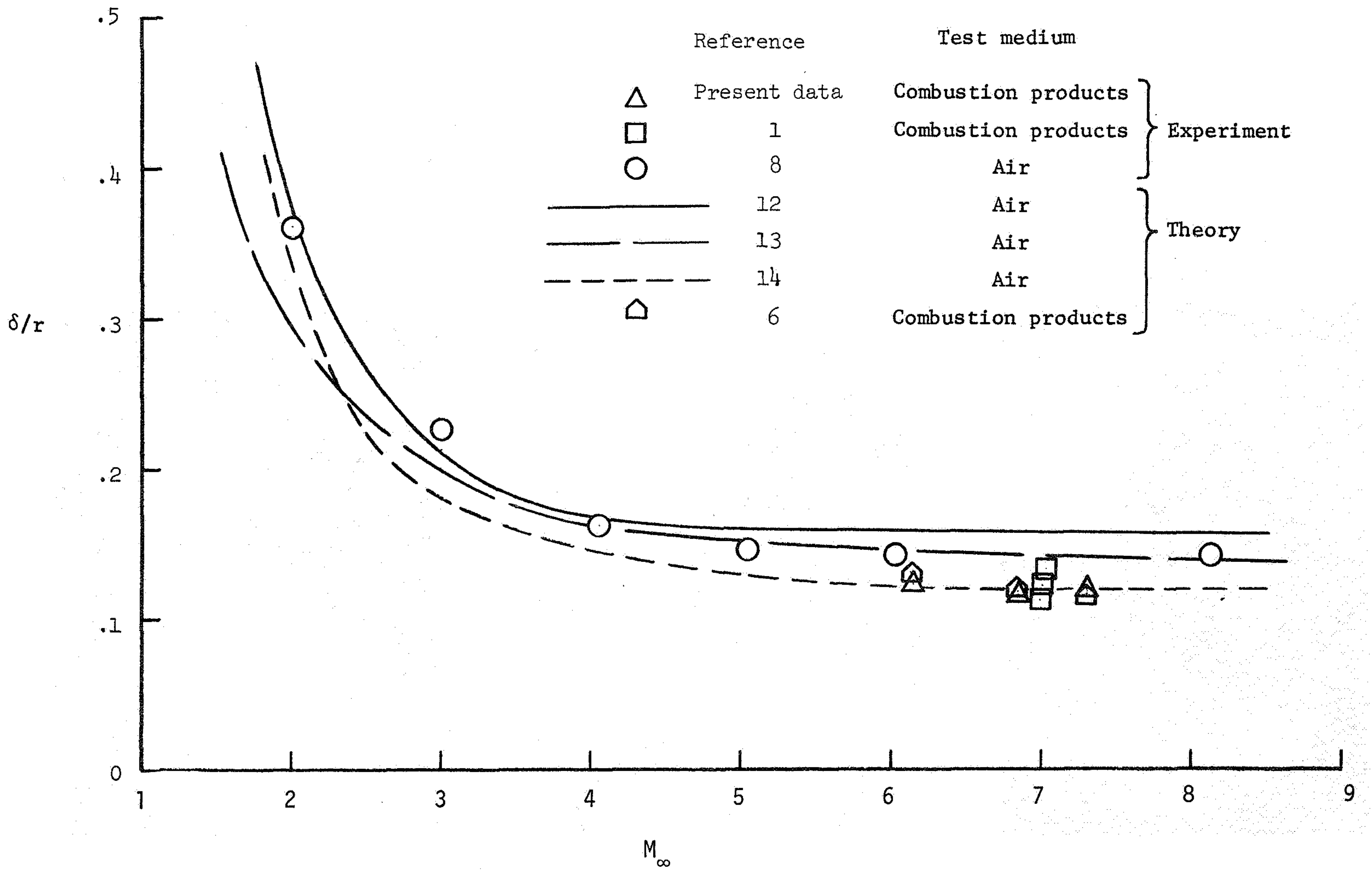

Figure 13.- Experimental and theoretical shock-wave standoff distances.

NASA-Langley, 1973 —— 33 L-8359

"The aeronautical and space activities of the United States shall be conducted so as to contribute . . . to the expansion of human knowledge of phenomena in the atmosphere and space. The Administration shall provide for the widest practicable and appropriate dissemination of information concerning its activities and the results thereof."

—NATIONAL AERONAUTICS AND SPACE ACT OF 1958

NASA SCIENTIFIC AND TECHNICAL PUBLICATIONS

TECHNICAL REPORTS: Scientific and technical information considered important, complete, and a lasting contribution to existing knowledge.

TECHNICAL NOTES: Information less broad in scope but nevertheless of importance as a contribution to existing knowledge.

TECHNICAL MEMORANDUMS: Information receiving limited distribution because of preliminary data, security classification, or other reasons. Also includes conference proceedings with either limited or unlimited distribution.

CONTRACTOR REPORTS: Scientific and technical information generated under a NASA contract or grant and considered an important contribution to existing knowledge.

TECHNICAL TRANSLATIONS: Information published in a foreign language considered to merit NASA distribution in English.

SPECIAL PUBLICATIONS: Information derived from or of value to NASA activities. Publications include final reports of major projects, monographs, data compilations, handbooks, sourcebooks, and special bibliographies.

TECHNOLOGY UTILIZATION PUBLICATIONS: Information on technology used by NASA that may be of particular interest in commercial and other non-aerospace applications. Publications include Tech Briefs, Technology Utilization Reports and Technology Surveys.

Details on the availability of these publications may be obtained from:

SCIENTIFIC AND TECHNICAL INFORMATION OFFICE

NATIONAL AERONAUTICS AND SPACE ADMINISTRATION

Washington, D.C. 20546